# Time and space correlation between sprites and their parent lightning flashes for a thunderstorm observed during the HyMeX campaign

S. Soula, E. Defer, M. Füllekrug, O. van Der Velde, J. Montanyà, Olivier Bousquet, J. Mlynarczyk, S. Coquillat, Jean-Pierre Pinty, W. Rison, et al.

▶ **To cite this version:**

S. Soula, E. Defer, M. Füllekrug, O. van Der Velde, J. Montanyà, et al.. Time and space correlation between sprites and their parent lightning flashes for a thunderstorm observed during the HyMeX campaign. Journal of Geophysical Research: Atmospheres, 2015, 120 (22), pp.11,552 - 11,574. 10.1002/2015JD023894 . hal-01717432

**HAL Id: hal-01717432**
**https://hal.science/hal-01717432v1**

Submitted on 3 Sep 2021

**HAL** is a multi-disciplinary open access archive for the deposit and dissemination of scientific research documents, whether they are published or not. The documents may come from teaching and research institutions in France or abroad, or from public or private research centers.

L'archive ouverte pluridisciplinaire **HAL**, est destinée au dépôt et à la diffusion de documents scientifiques de niveau recherche, publiés ou non, émanant des établissements d'enseignement et de recherche français ou étrangers, des laboratoires publics ou privés.

Copyright

AGU PUBLICATIONS

JGR

Journal of Geophysical Research: Atmospheres

RESEARCH ARTICLE
10.1002/2015JD023894

**Key Points:**
- The sprite-producing lightning flashes have a long propagation within the stratiform region
- The CMC of the stroke is confirmed as a good predictor of the sprite production
- Long-delayed sprites are associated with current moment waveforms of low amplitude and long duration

**Correspondence to:**
S. Soula,
sous@aero.obs-mip.fr

**Citation:**
Soula, S., et al. (2015), Time and space correlation between sprites and their parent lightning flashes for a thunderstorm observed during the HyMeX campaign, *J. Geophys. Res. Atmos.*, *120*, 11,552–11,574, doi:10.1002/2015JD023894.

Received 7 JUL 2015
Accepted 29 OCT 2015
Accepted article online 3 NOV 2015
Published online 27 NOV 2015

©2015. American Geophysical Union. All Rights Reserved.

# Time and space correlation between sprites and their parent lightning flashes for a thunderstorm observed during the HyMeX campaign

**S. Soula[1], E. Defer[2], M. Füllekrug[3], O. van der Velde[4], J. Montanya[4], O. Bousquet[5], J. Mlynarczyk[6], S. Coquillat[1], J.-P. Pinty[1], W. Rison[7], P.R. Krehbiel[7], R. Thomas[7], and S. Pedeboy[8]**

[1]Laboratoire d'Aérologie, Université de Toulouse, CNRS, UPS, Toulouse, France, [2]LERMA, Observatoire de Paris, CNRS, Paris, France, [3]Department of Electronic and Electrical Engineering, University of Bath, Bath, UK, [4]Electrical Engineering Department, Technological University of Catalonia, Terrassa, Spain, [5]LACy, UMR 8105, Météo-France/CNRS/Université de La Réunion, Saint-Denis, France, [6]Department of Electronics, AGH University of Science and Technology, Krakow, Poland, [7]NMT, Socorro, New Mexico, USA, [8]Météorage, Pau, France

**Abstract** During the night of 22–23 October 2012, together with the Hydrology cycle in the Mediterranean eXperiment (HyMeX) Special Observation Period 1 campaign, optical observations of sprite events were performed above a leading stratiform Mesoscale Convective System in southeastern France. The total lightning activity of the storm was monitored in three dimensions with the HyMeX Lightning Mapping Array. Broadband Extremely Low Frequency/Very Low Frequency records and radar observations allowed characterizing the flashes and the regions of the cloud where they propagated. Twelve sprite events occurred over the stratiform region, during the last third of the lightning activity period, and well after the coldest satellite-based cloud top temperature (−62°C) and the maximum total lightning flash rate (11 $min^{-1}$). The sprite-producing positive cloud-to-ground (SP + CG) strokes exhibit peak current from 14 to 247 kA, Charge Moment Changes (CMC) from 625 to 3086 C km, and Impulsive CMC (iCMC) between 242 and 1525 C km. The +CG flashes that do not trigger sprites are initiated outside the main convective core, have much lower CMC values, and in average, shorter durations, lower peak currents, and shorter distances of propagation. The CMC appears to be the best sprite predictor. The delay between the parent stroke and the sprite allows classifying the events as short delayed (<20 ms) and long delayed (>20 ms). All long-delayed sprites, i.e., most of the time carrot sprites, are produced by SP + CG strokes with low iCMC values. All SP + CG flashes initiate close to the convective core and generate leaders in opposite directions. Negative leaders finally propagate toward lower altitudes, within the stratiform region that coincides with the projected location of the sprite elements.

## 1. Introduction

Sprites constitute a type of Transient Luminous Events (TLEs) that are commonly observed from ground. They consist of streamer discharges, in response to a strong transient electrostatic field that exceeds the threshold for dielectric breakdown in the mesosphere [*Pasko et al.*, 1997], either rapidly (a few milliseconds) after the lightning stroke [*Bell et al.*, 1998; *Cummer and Lyons*, 2005] or a few tens of milliseconds after a long lightning continuing current following the stroke [*Cummer and Füllekrug*, 2001]. The sprite discharge can cover an altitude range from 40 to 90 km [*Sentman and Wescott*, 1993; *McHarg et al.*, 2002] and appear as various vertically structured shapes, individual or multiple column or/and carrot-shaped luminous elements [*Neubert et al.*, 2008; *van der Velde et al.*, 2006]. Sprites can also horizontally extend over several tens of kilometers in the form of sprite clusters [*Sentman et al.*, 1995; *Füllekrug et al.*, 2001; *Soula et al.*, 2014] and even over more than 100 km in the form of sequential luminous emissions that are called "dancing sprites" [*Winckler et al.*, 1996; *Füllekrug et al.*, 2013a].

Sprites are generally observed above the stratiform region of a Mesoscale Convective System (MCS) after positive polarity cloud-to-ground (SP + CG) strokes that lower a large amount of charge to the ground [*Boccippio et al.*, 1995; *Lyons*, 1996; *São Sabbas et al.*, 2003; *Cummer and Lyons*, 2005; *Soula et al.*, 2009]. Sprites are produced when the lightning activity associated with the convective regions of the storm decreases and when the stratiform region is well developed [*Soula et al.*, 2009; *Lang et al.*, 2010]. Most of the time, the SP + CG flashes start close to the convective cores and horizontally extend across the stratiform region with layers of alternating charge polarity at different altitudes. The flashes often extend from higher

altitudes in the convective core regions toward lower altitudes in the stratiform region and supposedly follow trajectories of ice particles toward the rear of the storm system [*Carey et al*., 2005; *Ely et al*., 2008; *van der Velde et al*., 2010, 2014]. Some of these flashes can be considered as spider lightning [*Mazur et al*., 1998; *Lang et al*., 2004]. Along their horizontal extent they can have several connections to the ground with positive and negative polarity [*Lang et al*., 2004; *Soula et al*., 2010].

In a recent work, *van der Velde et al.* [2014] analyzed the bidirectional development of several flashes associated with sprite production. They identified five modes of evolution of the negative leaders throughout the thundercloud system that explain the positioning and timing of the positive +CG strokes: #1 for slow bidirectional development with negative leader termination before the +CG stroke; #2 for fast bidirectional development with the negative leader continuing after the +CG stroke; #3 for slow-fast bidirectional development with a negative leader exhibiting a sudden lowering and speed increase; #4 for fast secondary bidirectional development from an in-cloud horizontal positive leader (in this case, the negative leaders propagate rapidly into the upper positive charge layer, continuing after the +CG stroke); #5 for slow bidirectional development with a long negative leader (50 km) subject to a cutoff while the original positive leader remained trapped inside negatively charged areas (in this case, a +CG stroke subsequently occurred under the old negative leader channel). They found that carrot sprites tend to be associated with fast extending leaders after the stroke and columniform/mixed sprites with slower side branches. Thus, the negative leaders may propagate at various altitudes and velocities, and over various distances, while positive leaders counterpart simultaneously propagate and determine the location of the +CG strokes. However, SP + CG flashes can be initiated in small convective cells, where they generally occur in the decaying convective region [*van der Velde et al*., 2010].

Time delays of sprites relative to the parent strokes can be very variable from $<$1 ms to more than 100 ms for some cases, even if the majority stays within 20 ms after the return stroke [*Hu et al*., 2002; *São Sabbas et al*., 2003; *van der Velde et al*., 2006; *Li et al*., 2008; *Montanyà et al*., 2010]. Sprites are often laterally displaced from the ground location of parent strokes, and the horizontal offset can vary from 0 to 100 km [*Sentman et al*., 1995; *Lyons*, 1996; *Füllekrug et al*., 2001; *São Sabbas et al*., 2003; *Matsudo et al*., 2009; *Soula et al*., 2010; *Lu et al*., 2013]. This is related to the geometry of the lightning channel and especially the tortuosity and the length of its horizontal section [*Fuquay*, 1982], which can have a significant influence on the sprite location above the storm. As a matter of fact, recent observations and modeling suggest that the intracloud (IC) component of SP + CG flashes could play a significant role in sprite formation [*Valdivia et al*., 1997; *van der Velde et al*., 2006, 2014; *Marshall et al*., 2007; *Asano et al*., 2009b]. For example, measurements have shown that at least in some cases, the IC components are connected to a simultaneous enhancement in cloud-to-ground charge transfer [*Li et al*., 2008], and modeling shows that this charge transfer can produce a sprite [*Yashunin et al*., 2007; *Asano et al*., 2009a]. Numerical modeling also shows that a horizontal in-cloud lightning channel might be the origin of sprites which are laterally displaced from their parent strokes and account thereby for some of the variance in sprite morphology [*Asano et al*., 2009b].

The sprite production could be also related to the presence of irregularities in the mesosphere [*Sentman et al*., 2003]. As a matter of fact, recent model calculations strongly suggest that enhancements of the electron density in the middle atmosphere are particularly effective in assisting the initiation of sprites below the conventional breakdown threshold [*Qin et al*., 2012, 2013; *Kosar et al*., 2012]. The initiation of sprites below the conventional breakdown threshold is currently under debate [*Liu et al*., 2009] based on numerous compelling observations and numerical simulations of sprites [*Gamerota et al*., 2011; *Li et al*., 2008; *Hu et al*., 2007]. Besides, *Füllekrug et al.* [2013b] reported the experimental detection of a large mesospheric irregularity which was probably illuminated by lightning electromagnetic fields at the altitude of sprite formation (80–85 km) after an intense positive cloud-to-ground lightning discharge that produced a sprite discharge in southern France.

Optical TLE observations are regularly performed from several stations in southern Europe. Numerous sprites and other TLEs have been observed above thunderclouds which develop from the beginning of May to the end of November [*van der Velde et al*., 2006; *Neubert et al*., 2008; *Soula et al*., 2009, 2010]. The typical characteristics of TLEs determined in other regions of the world are also observed in cases detected in southern and central France during the summer season and along the Mediterranean coastline during the fall season. Case studies in Europe allow us to distinguish some relationships between the type of sprite, the time delay of sprite production after the parent CG flash [*van der Velde et al*., 2006; *van der Velde*, 2008], and specifics of the lightning activity associated with sprite production and CG flash sequences [*Soula et al*., 2010].

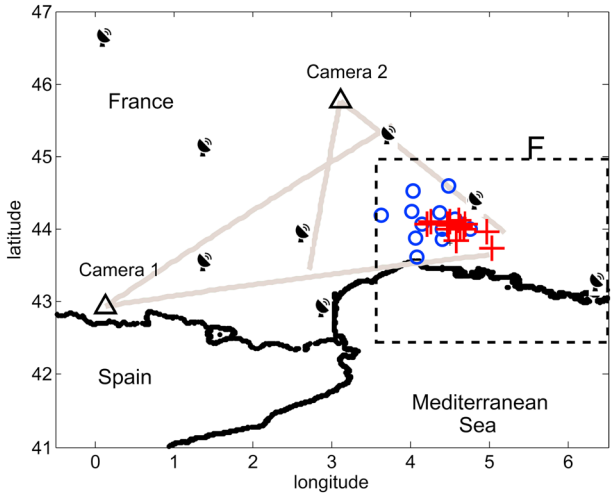


**Figure 1.** Location and geometry of the FOV of both video cameras, location of the radars of the French network ARAMIS (radar symbols), the 12 SP + CG flashes (red crosses), and location of the 12 LMA stations (blue circles). The dashed line frame F indicates the area where the storm activity is analyzed.

Electromagnetic (EM) emissions associated with sprites can provide information about their current characteristics and their specific signatures for their identification [*Cummer et al.*, 1998; *Füllekrug et al.*, 2001]. *Reising et al.* [1996] showed that sprite-producing +CG lightning flashes produce large extremely low frequency (ELF) tails following the initial VLF portion, indicating the presence of continuing current in the discharge. Radio waveforms in the ELF range (from 3 Hz to 3 kHz) originating in sprite-producing lightning discharges have been used to estimate the charge removed [*Cummer and Inan*, 1997; *Bell et al.*, 1998]. *Cummer et al.* [1998] presented the first evidence of electrical current within the body of sprites by identifying magnetic field waveforms in the ELF range coinciding with sprites. *Stanley et al.* [2000] detected electric-field change waveforms that showed very large sprites occurred daytime. More recent work shows that radio waves in the ELF range could be produced by sprites [*Füllekrug et al.*, 2001; *Rycroft and Odzimek*, 2010] and that these specific signatures could be used for estimating the sprite rate at the Earth surface [*Ignaccolo et al.*, 2006].

The HYdrological cycle in the Mediterranean EXperiment (HyMeX) project is a 10 year project dedicated to the study of the hydrological cycle and related high-impact events [*Drobinski et al.*, 2014]. As detailed in *Ducrocq et al.* [2014], the first Special Observation Period (SOP1) campaign of this project was conducted during 2 months (6 September 2012 to 5 November 2012) over the Northwestern Mediterranean Sea and its coastal regions in France, Italy, and Spain. The instrumental and observational strategy of the SOP1 campaign was set up to document and improve the knowledge on atmospheric processes leading to heavy precipitation and flash flooding in that specific Mediterranean region. The PEACH (Projet en Electricité Atmosphérique pour la Campagne HyMeX) project is the Atmospheric Electricity component of HyMeX. It is dedicated to the observation of both lightning activity and the electrical state of continental and maritime thunderstorms in the area of the Mediterranean Sea. During the HyMeX SOP1, four European operational lightning locating systems (ATDNET, EUCLID, LINET, and ZEUS) and the HyMeX Lightning Mapping Array (HyLMA) were used to locate and characterize the lightning activity over the Southeastern Mediterranean at the scale of individual flashes and storms and at regional scale [*Defer et al.*, 2015]. During the night of 22–23 October 2012, sprite production and lightning activity were simultaneously monitored while a storm developed close to the coastline of the Mediterranean Sea and over the area covered by the HyLMA.

The set of the data available allows us to investigate several issues related to physics of sprites and lightning flashes, especially the following points that will be discussed: (i) the relationships between the characteristics of the SP + CG flashes and those of the sprites, (ii) the triangulated sprite location and the flash leader developments, (iii) the altitudes of positive charge removal by the SP + CG flashes, (iv) the origins and characteristics of negative and positive leaders and their relation to the sprites as reported by *van der Velde et al.* [2014]. The different sensors and data acquisition systems are presented in section 2. Section 3 describes the observations in a global perspective. Section 4 is devoted to a detailed case study at the lightning flash scale. A discussion is proposed in section 5, and finally a conclusion section summarizes the main points of the study.

## 2. Observations

### 2.1. Optical Observations

The system for the optical observation of TLEs used during the night of 22–23 October consisted of two video cameras installed at Pic du Midi (42.93°N, 0.14°E; 2877 m) and at Clermont-Ferrand (45.76°N, 3.11°E; 400 m), as

indicated in Figure 1 with cameras 1 and 2, respectively. Both cameras are low-light Watec 902H (minimum illumination of 0.0001 lux) with a high-resolution charge-coupled device. They are mounted on a pan-tilt unit remotely controlled via the Internet. Cameras 1 and 2 have fields of view (FOV) of 31° and 47°, respectively, indicated in Figure 1 with grey lines, as they were oriented at the time of the observation. They operate in a trigger mode defined by the UFOCaptureV2 software (http://sonotaco.com/soft/e_index.html#ufocv2, accessed date) in order to capture sprites with brightness above a given threshold. Videos are saved at a rate of 25 frames (or 50 interlaced fields) per second, which provides a time resolution of 20 ms. The GPS-referenced time is inserted in the video imagery.

Azimuth and elevation of the sprite events can be determined by using the software "Cartes du Ciel" (SkyCharts) as described in *van der Velde* [2008]. This software allows us to overlay known stars on an image from the video imagery, given a certain time, location, and fraction of the sky. The matching of the stars with those in the image is done manually. This method works very well if the camera direction and observation time are known and enough stars are visible. For a sprite event, the azimuths are determined for one or several elements according to the number of elements that compose the event. If the sprite event is detected by two cameras, this azimuth determination is made for both images and the triangulation allows determining the area of sprite occurrence. Actually, with a 20 ms resolution in the video imagery it is difficult to triangulate individual sprite elements. A sprite is usually much wider than the readout of azimuth, which varies typically only within 0.17°. The uncertainty of the triangulation for an event at 300 km distance is smaller than 1 km. Altitude calculations are not used in this study.

### 2.2. Lightning Detection

The CG flashes were recorded with the European lightning detection network operated by European Cooperation for Lightning Detection (EUCLID). It allows identifying the location, polarity, peak current, and the timing of CG strokes. CG flashes are reconstructed from the strokes with time and space criteria of 0.5 s and 10 km, respectively [*Cummins et al*., 1998]. All sensors use both magnetic direction finding and time-of-arrival techniques to determine the location of CG strokes [*Cummins et al*., 1998]. The detection efficiency is ~90% over land and close to the coastline. In the present study, both individual strokes and CG flashes are considered, according to the requirements of the study.

The lightning structure within the electrified thunderclouds including negative and positive leaders is determined with the Lightning Mapping Array (HyLMA) deployed and managed by New Mexico Tech [*Rison et al*., 1999; *Thomas et al*., 2004] during the field experiment of HyMeX in southeastern France. This HyLMA was composed of 12 ground-based receivers using the "time-of-arrival" technique [*Proctor*, 1971] to locate in 3-D the VHF emissions produced by stepped negative and positive leaders (see Figure 1). It was equipped with GPS synchronization to locate individual very high frequency (VHF) sources in successive 80 μs time windows [*Rison et al*., 1999*; Defer et al*., 2015]. The negative leaders developing through positively charged cloud regions are more impulsive than the positive leaders developing through negatively charged regions, and thus, they produce more VHF sources allowing the LMA system to infer the gross charge structure of thunderclouds [*Bruning et al*., 2010]. Different phases of the lightning flashes can be distinguished and associated with other characteristics of the storm activity. In the present study, the storm was located more or less directly above the 12 HyLMA stations (a square of approximately 100 km × 100 km) when the sprites were detected by the two cameras. In fact, the SP + CG strokes are located within 100 km of the HyLMA origin (Figure 1), and therefore, the HyLMA detection efficiency was high according to previous reports [*Thomas et al*., 2004; *Lang et al*., 2010]. The HyLMA data are considered and analyzed in detail when they are located by ≥8 VHF receivers with reduced chi-square ($\chi^2$) values ≤ 1.

### 2.3. Broadband EM Emissions and Charge Moment Changes

Observations of broadband ELF/VLF/LF/MF activity have been performed with a system located at University of Bath (51.71°N, 2.32°W; ~1200 km from the storm location). It consists of a wideband digital low-frequency radio receiver described in *Füllekrug* [2010]. The system includes a metal plate insulated from the ground to measure the vertical electric field, a precise GPS clock for timing the data acquisition, and an analogue signal conditioning and digital data acquisition unit. This instrument has the capability to record electric field magnitudes in the frequency range from approximately 4 Hz to 400 kHz with a sampling frequency of 1 MHz, and an amplitude resolution of ~35 μV m$^{-1}$ and a timing accuracy of ~12 ns.

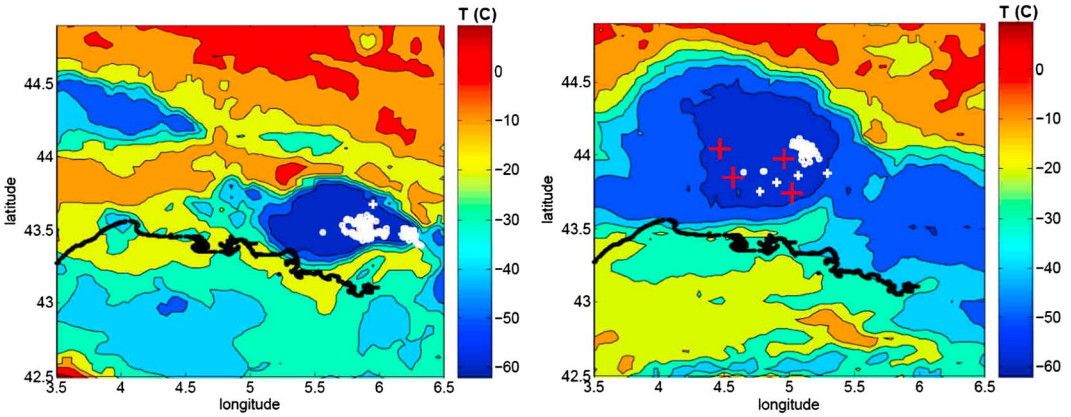


**Figure 2.** Cloud top temperature from MSG satellite in the frame F of Figure 1: (left) at 2140 UTC on 22 October and (right) at 2325 UTC on 22 October. Locations of −CG (white circles), +CG (white crosses), and SP + CG (red crosses) detected over 20 min around the scan time are superimposed.

The charge moment change (CMC), the impulsive CMC (iCMC), and the current moment waveform associated with the CG flashes [*Hu et al*., 2002; *Cummer and Lyons*, 2005] were reconstructed from ELF receiver measurements, by using the method presented by *Mlynarczyk et al.* [2015]. The ELF recordings were made by the Hylaty ELF station in Poland [*Kulak et al*., 2014].

### 2.4. Cloud Structure and Characteristics

Reflectivity from the French meteorological radar network ARAMIS ("Application Radar à la Météorologie Infra-Synoptique") is used to describe the structure of the storm. ARAMIS consists of 24 Doppler radars (C band and S band) that cover the entire area of mainland France and Corsica [*Bousquet and Tabary*, 2014]. The study area is covered by eight radars whose data were combined to reconstruct 3-D fields of radar reflectivity every 15 min up to a height of 14 km above mean sea level. The horizontal (respectively, vertical) resolution of reflectivity fields is 1 km (respectively, 0.5 km). More details about the particular radar setup used during HyMeX can be found in *Bousquet et al.* [2014].

The cloud top temperatures are provided by the Meteosat satellite from European Organization for the Exploitation of Meteorological Satellites. Meteosat Second Generation (MSG) Spinning Enhanced Visible and Infrared Imager is based on radiometer data in the thermal infrared band at 11–13 μm. The temperature accuracy is generally better than 1 K. The parallax error (evaluated to about 15 km at this latitude for a cloud top at 12 km) is taken into account for the plots which associate the locations of CG strokes with their parent clouds (Figure 2).

## 3. Overview of Storm Activity and Sprite Observation

On 22 October 2012, a low-pressure area located over the Balearic Islands and a high-pressure area over Central Europe organized a southeasterly flow that carried unstable air over southeastern France and Mediterranean regions. This instability favored the storm development in a large part of the country during the day, and the instability was localized along the eastern Mediterranean coastline at the end of the day. Moderately large CAPE values were reported, as for example ~900 J kg$^{-1}$ from a sounding in Ajaccio (Corsica) on 22 October at 1200 UT. During the evening, a storm developed in southeastern France and moved in a west-northwest direction as illustrated in Figure 2 with the distribution of the cloud top temperature recorded with the infrared radiometer on board the MSG satellite at 2140 and 2325 UTC (times of the scan over the storm region). The spatial extent of the active part of the thundercloud grew relatively quickly during more than 1 h and reached approximately 200 km in length and 100 km in width at 2325 UTC. The CG lightning activity is displayed in this figure by use of the locations of +CG and −CG strokes detected during 20 min centered on the time of the thundercloud scan. The SP + CG strokes are also indicated in the graph at 2325 UTC. Most of the CG strokes were located in a restricted area of the cloud system, probably related to the convective region, especially at 2140 UTC. At 2325 UTC, the strokes were overall less numerous and more scattered.

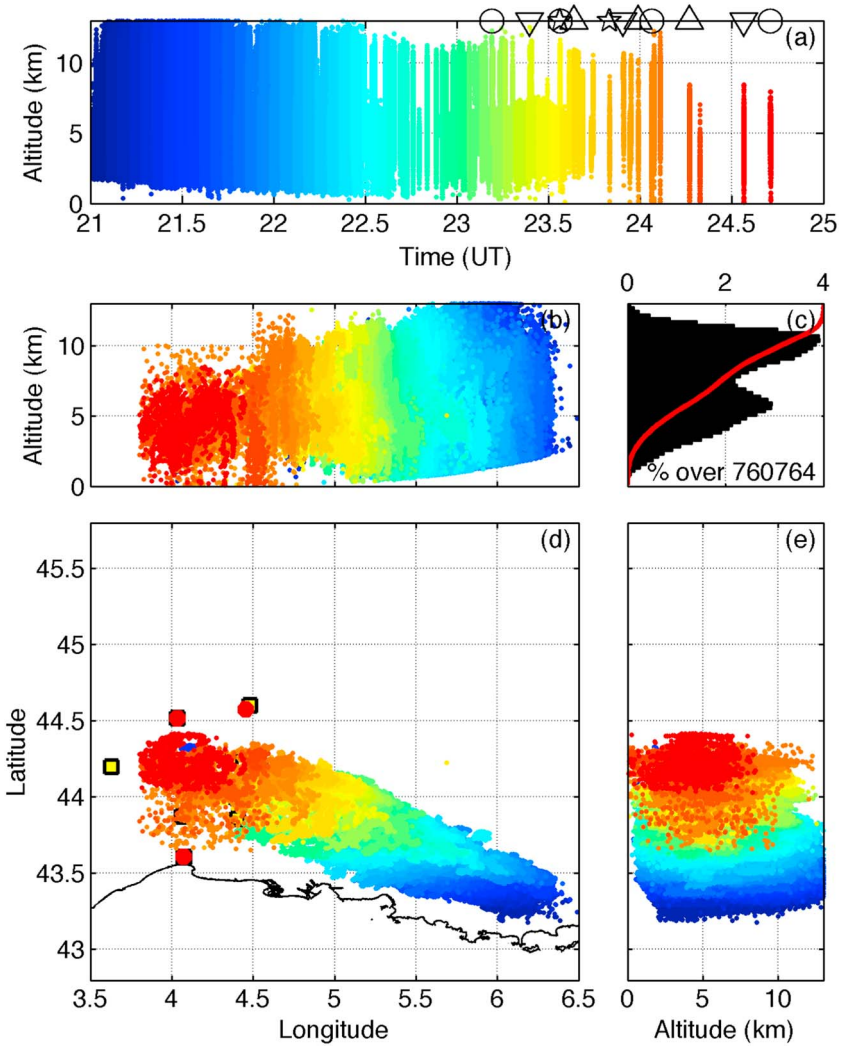


**Figure 3.** VHF detections from the HyLMA between 2100 UTC on 22 October and 0100 UTC on 23 October above the same area as Figure 2. (a) Time series of the VHF source altitude with the sprite events indicated by symbols (circle for column, inverted triangle for carrot, star for jellyfish, and triangle for wishbone), (b) altitude of VHF sources versus the longitude, (c) vertical profile of VHF source density, (d) 2-D geographical distribution of VHF sources, and (e) latitude versus altitude for VHF sources. The color indicates the time window.

The total lightning activity was monitored by the HyLMA system, the stations of which are indicated by blue squares in Figure 1. It is described with different graphs in Figure 3 for a period of about 4 h between 2100 UTC and the end of the lightning activity around 0045 UTC on 23 October, in Figure 4 for a shorter period of 2 h starting at 2300 UTC. Figures 3a and 4a display the time series of the VHF source altitude with the sprite events indicated by symbols (circle for column, triangle for carrot, star for jellyfish, and inverted triangle for wishbone). The time is expressed in hour with decimal values. Figures 3b and 4b display the altitude of VHF sources versus the longitude, Figures 3c and 4c the vertical profile of VHF source density, Figures 3d and 4d the 2-D geographical distribution of VHF sources, and Figures 3e and 4e the latitude versus the altitude of VHF sources. The color indicates the time window. A maximum of VHF sources is observed around 10 km in altitude during the first period of the storm activity as indicated in Figures 3a, 4a, 3c, and 4c. It means that during the most active period, the charge structure of the thundercloud corresponds to a normal dipole with a positive charge above a negative one. On the contrary, during the last 2 h, a maximum of VHF sources is observed around 5 km in altitude, which means that the positive charge was prominent at lower altitude. While at 2100 UTC the storm activity was at a distance of about 150–180 km to the HyLMA, the final activity was above it and weak (Figures 3d and 4d).

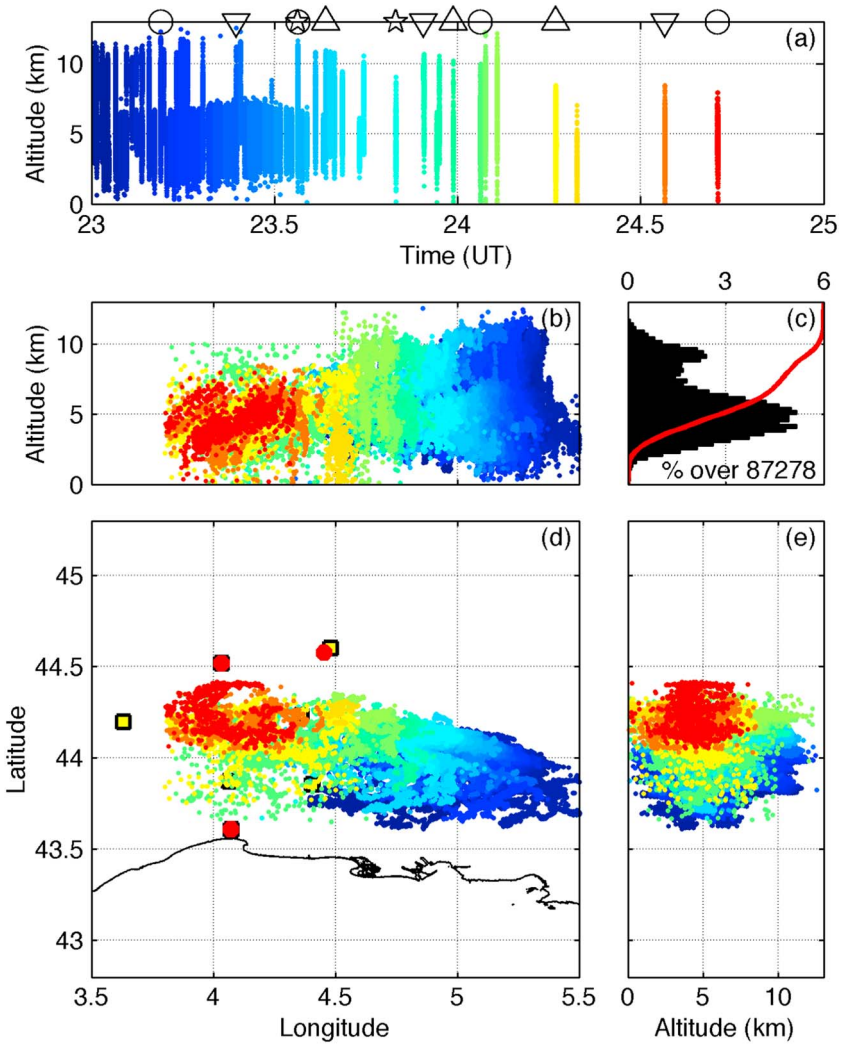


**Figure 4.** Same as Figure 3 for HyLMA detections between 2300 UTC on 22 October and 0100 UTC on 23 October above a little more restricted area.

The combination of HyLMA and Euclid data allows analyzing the lightning activity in terms of CG and IC flash characteristics. Figure 5a displays the temporal distribution of the peak current values for all CG strokes detected between 2100 UTC and 0100 UTC. This graph displays also the area with a temperature of cloud top lower than −40°C (A(−40)) and the minimum temperature of the cloud top versus time. The lowest temperature of the cloud top (−62 °C) is reached at 2130 UTC when the CG lightning activity is high compared to the whole period and subsequently it warms to about −52 °C at 0100 UT on 23 October, indicating a decrease in cloud top altitude. According to the evolution of A(−40), the size of the cloud system increases continuously between 2100 and 2230 UTC, then stabilizes below and close to 30,000 $km^2$ during about 1 h, and decreases after 2330 UTC. The first sprite events are produced during this stabilization of A(−40). At the end of the CG lightning activity, most +CG flashes detected are classified as SP + CG flashes. Figure 5b displays the time series of the rates of different types of flash (total flashes, IC flashes, and CG flashes) and the proportion of CG flashes. The lightning activity increases rapidly after 2100 UTC with a maximum of the total flash rate around 11 flashes per minute at 2110 UTC, then it decreases rapidly, especially for the IC flashes the rate of which reaches very low values at 2150 UTC. The proportion of CG flashes increases progressively but irregularly during the sequence, reaches 100% at the beginning of the period of sprite observation, decreases for a few tens of minutes, and definitively maintains at 100% after 0010 UTC. The sprite production corresponds with a low IC flash rate and a large CG proportion. Figure 5c shows the westward displacement of the lightning activity ending with a majority of SP + CG flashes. As a matter of fact,

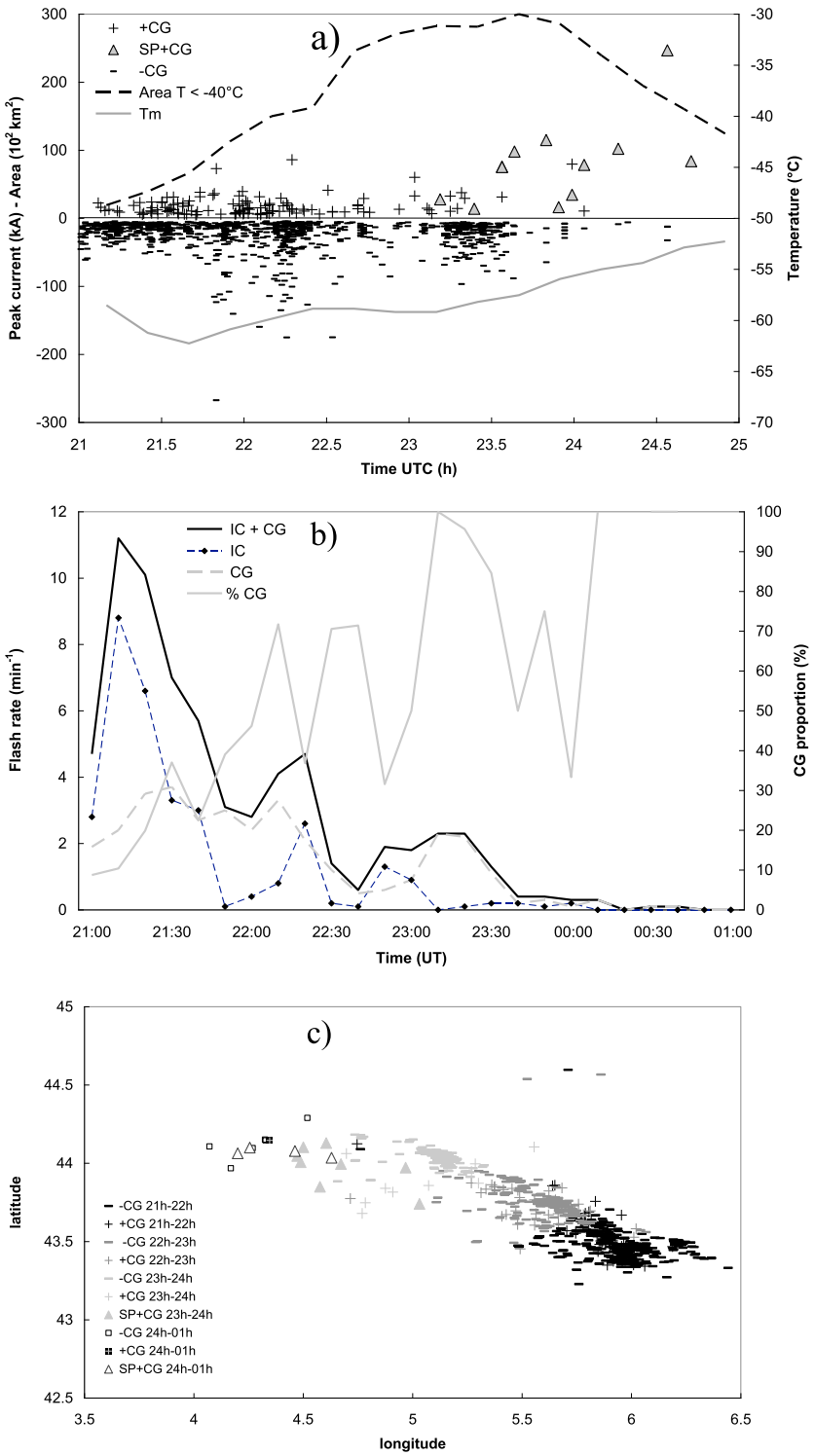


**Figure 5.** (a) Time series of the peak current of the CG strokes located in frame F of Figure 1, the area with a temperature of cloud top lower than −40°C (dashed line), and the minimum value of the cloud top temperature (solid line). (b) Time series of the flash rates and the CG flash proportion for the same domain and the same period. (c) Location of the same CG strokes (plus for +CG, minus for −CG, and triangle for SP + CG) hour by hour with different levels of tone grey.

**Table 1.** Characteristics of the 12 TLE Events[a]

| Sprite Event | | | | | SP + CG Stroke | | | | | |
|---|---|---|---|---|---|---|---|---|---|---|
| | Time of First Frame (UTC) | | | | | | | | | |
| # | hh:mm | Cam 1 (s) | Cam 2 (s) | Type | Time (s) | Distance Cam 1 / Cam 2 (km) | Peak Current (kA) | $\Delta t$ Sprite (ms) | CMC (C km) | iCMC (C km) |
| 1 | 23:11 | 19.382 | - | col.[b] | 19.386 | 406/271 | 28 | 0–16 | 702 | 255 |
| 2 | 23:23 | 46.150 | - | car.[c] | 46.112 | 407/247 | 14 | 38–58 | 3086 | 156 |
| 3a | 23:33 | 50.316 | 50.309 | jel.[d] | 50.323 | 371/218 | 76 | 0–6 | 2980 | 1525 |
| 3b | 23:33 | 50.456 | 50.469 | col.[b] | 50.448 | 373/243 | 75 | 21–28 | 1300 | 398 |
| 4 | 23:38 | 23.798 | 23.797 | wis.[c] | 23.800 | 384/217 | 98 | 0–17 | 2806 | 898 |
| 5 | 23:49 | 56.085 | 56.079 | jel.[d] | 56.098 | 371/224 | 115 | 0–7 | 2348 | 1387 |
| 6 | 23:54 | 27.588 | 27.588 | car.[b] | 27.573 | 375/215 | 16 | 15–35 | 1629 | 242 |
| 7 | 23:59 | 18.511 | - | wis.[b] | 18.521 | 384/233 | 35 | 0–10 | 783 | 336 |
| 8 | 00:03 | 44.233 | 44.225 | col.[b] | 44.240 | 383/227 | 78 | 0–5 | 625 | 392 |
| 9 | 00:16 | - | 06.389 | wis.[c] | 06.404 | 372/216 | 116 | 0–5 | 2115 | 728 |
| 10 | 00:33 | 57.711 | 57.703 | car.[b] | 57.694 | 356/206 | 247 | 17–29 | 1840 | 352 |
| 11 | 00:42 | - | 36.199 | col.[b] | 36.207 | 351/208 | 84 | 0–12 | 1244 | 423 |

[a]For optical events: timing for each camera, type of TLE. For each SP + CG stroke: time, distance at each camera, peak current, delay of the sprite, CMC and iCMC. The type of sprite is indicated according to the classification by *Bór* [2013] and corresponding to the dominant type when several are present (col. for column, car. for carrot, jel. for jellyfish, and wis. for wishbone). The footnotes b to d indicate a subjective level of brightness.
[b]For low luminosity.
[c]For bright.
[d]For very bright.

during the first 1 hour interval (2100–2200 UTC) the strokes (black symbols) are located in the eastern region of the storm activity (5.5°E–6.5°E in longitude) and during the two last intervals (2300–0100 UTC) they are located in the western region (4°E–5.2°E in longitude).

During about 90 min of that period (2311 UTC to 0042 UTC), cameras 1 and 2 recorded nine videos and eight videos with sprites respectively, where six events were simultaneously recorded on both cameras. Thus, a total of 11 different videos including 12 sprite events were recorded. One video contains two sprite events and two videos contain sprite-associated halos. Table 1 reports the timing and the main characteristics of these events and those of their SP + CG strokes. The SP + CG strokes recorded by Euclid are also reported in Figure 1 with red crosses. They were located at distances between roughly 351 and 407 km from camera 1 and between 206 km and 271 km from camera 2. The peak currents of these SP + CG strokes range from 14 to 247 kA with an average value of 81 kA.

The time delay $\Delta t$ for the sprite production after the SP + CG stroke is reported in the last column of Table 1 as a time interval because of the uncertainty related to the timing of the sprite event (±20 ms, i.e., the duration of a video frame). However, according to the number of videos for an event (1 or 2), and according to the timing of the first video frame with sprite luminosity, this uncertainty is variable. Figure 6 illustrates the methodology of the general calculation of this time interval when the event is observed with two cameras. According to this scheme, the real time interval between the SP + CG stroke and the sprite event is the difference ($t_s - t_0$). With the uncertainty of ± 20 ms on $t_s$, the delay determined from the dual observations is included in the time interval $[t_1; t_2]$:

with $t_1 = t_{b1} - t_0$ and $t_2 = t_{e2} - t_0$

if $t_{b1} > t_{b2}$ and $t_0 > t_{b1}$

with $t_1 = 0$ if $t_0 > t_{b1}$

or,

with $t_1 = t_{b2} - t_0$ and $t_2 = t_{e1} - t_0$

if $t_{b2} > t_{b1}$ and $t_0 > t_{b2}$

with $t_1 = 0$ if $t_0 > t_{b2}$

All parameters are defined in the caption of Figure 6.

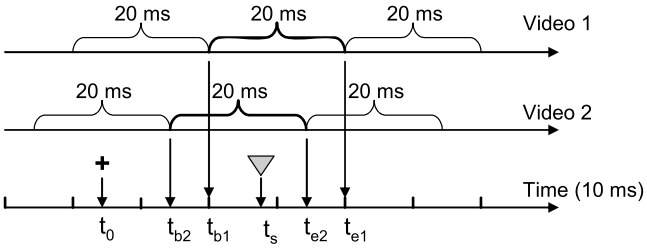


**Figure 6.** Diagram for the calculation of the time interval for the delay between the SP + CG stroke (plus) and the sprite event (grey triangle). The timings of the first video frames (bold braces) with sprite luminosity in each video are $t_{b1}$ and $t_{b2}$ for the beginning, $t_{e1}$ and $t_{e2}$ for the end. The duration of the frames in the video imagery is 20 ms.

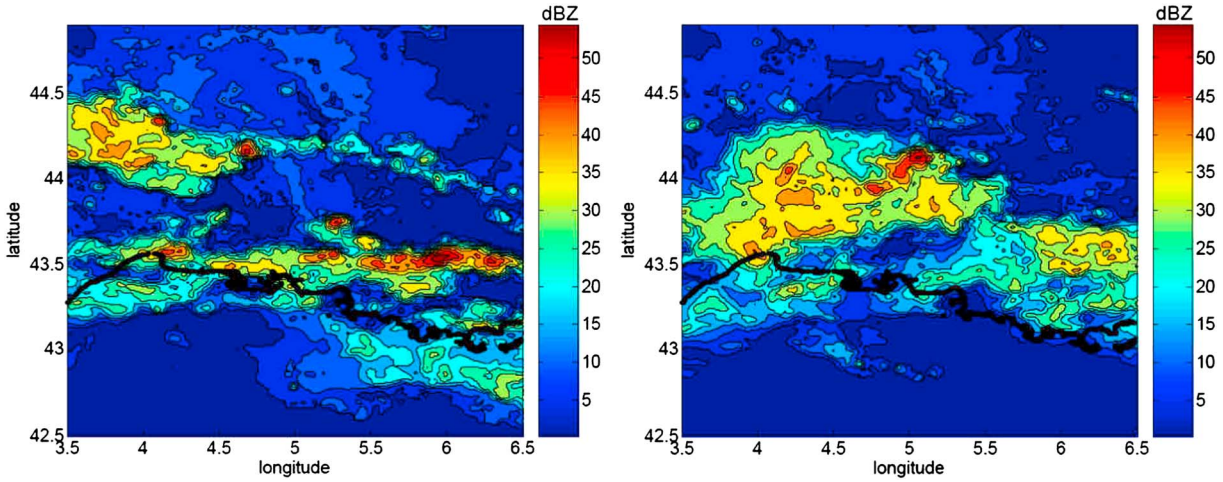


**Figure 7.** Multiple-Doppler analysis of radar reflectivity at an altitude of 3 km (left) at 2130 UTC and (right) at 2330 UTC. The frame corresponds to that of Figure 2.

The delays between the SP + CG strokes and the luminous emissions are included in a relatively large range of values since the maximum value $t_2$ ranges between 5 and 58 ms. The 12 intervals can be easily separated into two groups, a group of 8 events with $t_1 = 0$ that we consider as events with a short delay and a group of 4 events with $t_2 > 20$ ms that we consider as events with a long delay. The sprite events are classified in different types and a tendency appears which shows that the short-delayed events are either the column type or the jellyfish type or the wishbone type, while the long-delayed events are more often the carrot type.

Table 1 includes in the two last columns the CMC and iCMC values, respectively, for each stroke producing a sprite. It reveals a wide range of values for both parameters, since the CMC ranges from 625 to 3086 C km and the iCMC ranges from 156 to 1525 C km. It appears that there is no correlation between each of the parameters that characterize the SP + CG strokes, in terms of peak current, time delay $\Delta t$, CMC, and iCMC. As a matter of fact, a low or high value of each can be associated with a low or high value of each other. A detailed analysis of all these parameters will be developed in the following sections, in the framework of detailed case studies and in the discussion where characteristics of SP + CG flashes and +CG flashes produced during the same period of the storm will be compared.

Figure 7 displays a horizontal cross section of the radar reflectivity pattern at an altitude of 3 km for the same frame and for the same scanning times as in Figure 2. By comparing Figure 2 for CG lightning stroke location and Figure 7 for the storm structure, it is clear that the CG lightning strokes around 2130 UTC were mainly produced in a restricted area corresponding to the convective region with reflectivity values ranging around 50 dB*Z* and centered around (5.9°E, 43.5°N). At 2130 UTC the storm was organized in a convective line with several cells, two of them producing the stroke clusters displayed in Figure 2. Two hours later, the storm system has moved westward and the structure has changed. In fact, the size of the convective region was substantially reduced and the maximum value of the radar reflectivity decreased to 45 dB*Z*. The most significant change is the development of a large stratiform region ahead of the convective core with a reflectivity ranging between 25 and 40 dB*Z*. The CG strokes produced around 2140 and 2325 UT displayed in Figure 2 correspond to both types of region of the storm system: concentrated strokes in the convective region and scattered strokes, including some SP + CG strokes, in the stratiform region.

## 4. Case Studies of Sprite/Lightning Timing and Location

Figures 8–11 display graphs and pictures related to several sprite events as follows: (a) the longitude of HyLMA-detected VHF sources and Euclid-detected CG strokes versus time; (b) the altitude of HyLMA-detected VHF sources versus time; (c) the electric field radiated in the ELF/VLF/LF/MF range (for top/middle/bottom graphs) versus time during a short period around the sprite event (20 ms before to 100 ms after the sprite); (d) frames with sprite luminosity from the video imagery recorded by one or both cameras; (e) Radar reflectivity field at an altitude of 3 km with several events of the lightning activity associated with the sprite

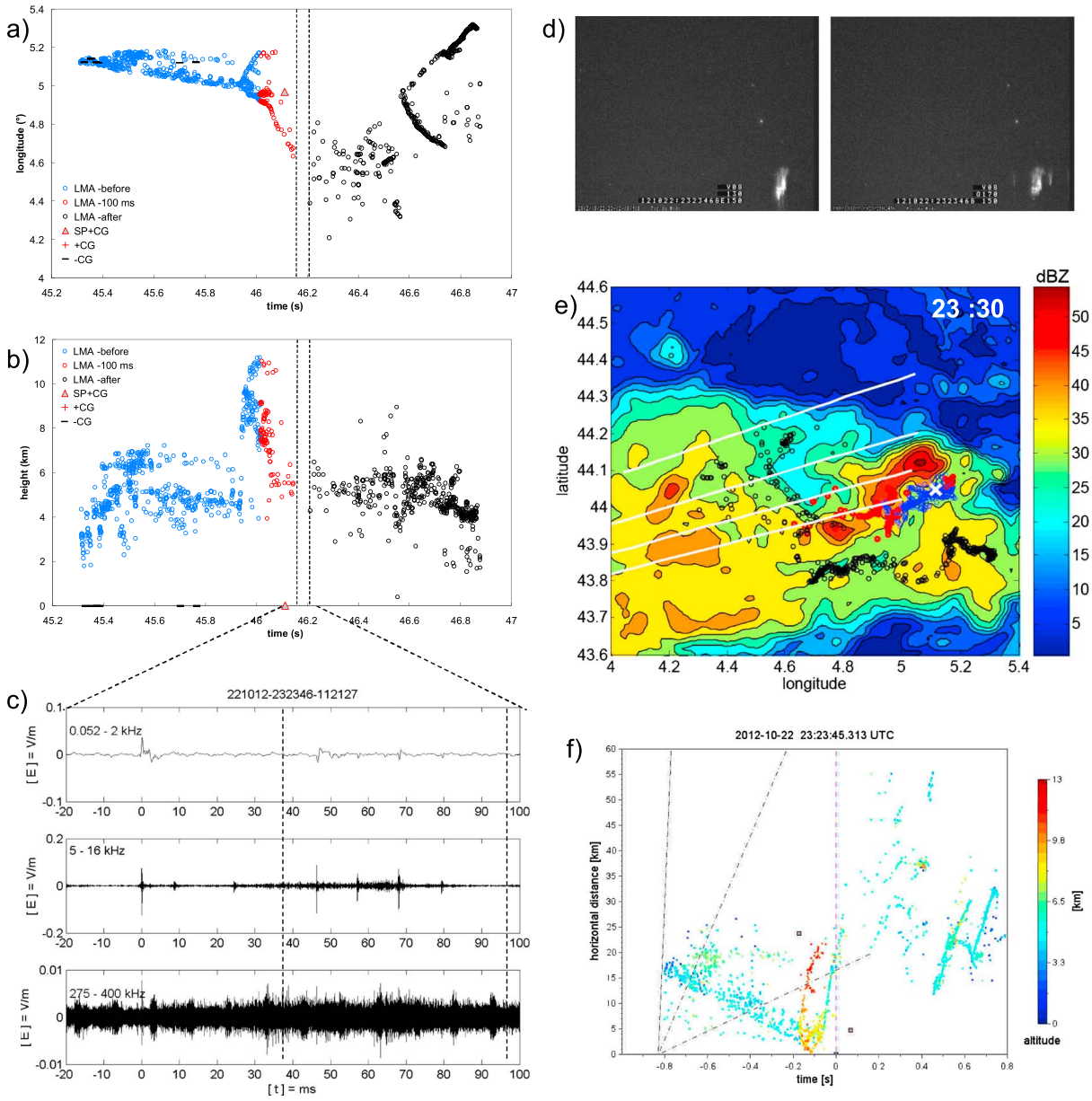


**Figure 8.** Long delay sprite (event #2 at 2323:46 UTC): (a) the longitude of HyLMA-detected VHF sources and Euclid-detected CG strokes versus time after 2323 UTC; (b) the altitude of HyLMA-detected VHF sources versus time after 2323 UTC; (blue/red/black for at least 100 ms before/less than 100 ms before/after sprite event). In Figures 8a and 8b the dashed lines display the time interval (multiple of 20 ms) with sprite luminosity in the video imagery. (c) the electric field radiated in ELF/VLF/LF range (for top/middle/bottom graphs) versus time during a short period around the sprite event (20 ms before to 100 ms after); (d) two successive frames with sprite luminosity from the video imagery recorded by camera 1 between $t = 46.150$ s and $t = 46.190$ s; (e) radar reflectivity field at the altitude of 3000 m at 2330 UTC, with superimposed several events of the lightning activity associated with the sprite: the HyLMA-detected VHF sources, the Euclid-detected CG strokes (the white cross indicates the first VHF source detected, and the white lines display the lines of sight of the main sprite elements); (f) time-distance graphs of the VHF sources, mapped by the HyLMA where the dashed reference lines indicate slopes corresponding to speeds of $2 \times 10^4$ m s$^{-1}$, $10^5$ m s$^{-1}$, and $10^6$ m s$^{-1}$. The SP + CG stroke is chosen as reference point for the distance (at $t = 0$). Black squares are stroke detections.

superimposed: the HyLMA-detected VHF sources (blue, red, and black circles), the Euclid-detected CG strokes (red crosses for +CG and blue squares for −CG). In this graph the white cross indicates the first reconstructed VHF source detected, and the white lines display the lines of sight of the edges of the sprite luminosity from both cameras. In Figures 8a, 9a, 10a, 11a, 8b, 9b, 10b, and 11b the dashed lines display the time interval (in multiple of 20 ms) with the sprite luminosity in the video imagery. For Figures 8a, 9a, 10a, 11a, 8b, 9b, 10b, 11b, 8c, 9c, 10c, and 11c which display the HyLMA-detected VHF sources, blue, red, and black correspond

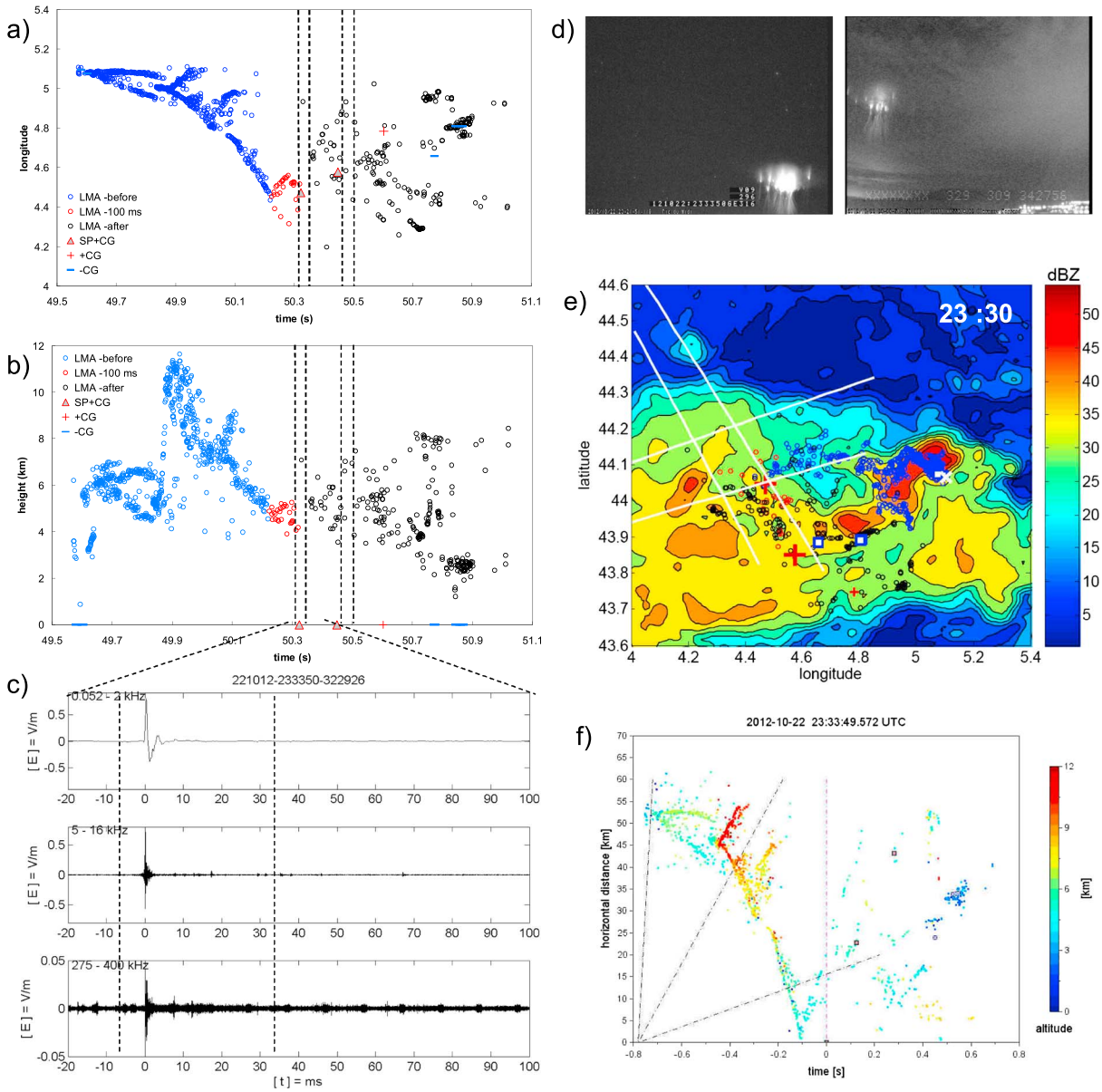


**Figure 9.** As in Figure 8 for a short delay sprite (event #3 at 2333:50 UTC). In Figure 9a and 9b time is after 2333 UTC. In Figure 9d two frames with sprite luminosity: (left) from camera 1 at $t = 50.316–336$ s and (right) from camera 2 at $t = 50.309–329$ s. In Figure 9e the reflectivity radar field is at 2330 UTC. In Figure 9f the SP + CG stroke is chosen as reference point for the distance (at $t = 0$).

to sources recorded at least 100 ms before, less than 100 ms before, and after the sprite event, respectively. Figures 8f, 9f, 10f, and 11f display time-distance of the VHF sources mapped by the HyLMA, as described in *van der Velde and Montanyà* [2013] for data from the Ebro LMA. In this graph, the dashed reference lines indicate slopes corresponding to speeds of $2 \times 10^4$ m s$^{-1}$, $10^5$ m s$^{-1}$, and $10^6$ m s$^{-1}$ and the reference location for the distance (at $t = 0$) is the SP + CG stroke.

### 4.1. Case of a Long Time-Delayed Sprite at 2323:46 UTC

Figure 8 corresponds to a long time-delayed sprite event at 2323:46 UTC (#2 in Table 1). According to Figures 8a and 8b, the first sequence of VHF sources (blue dots) starts at $t = 45.313$ s, lasts about 0.6 s, and corresponds to several propagations, some vertical and other horizontal. According to Figure 8b, some leaders propagate downward and are associated with four −CG strokes occurring rapidly between 45.328 and 45.385 s and exhibiting peak currents of −38, −43, −16, and −11 kA, respectively. The vertical velocity can

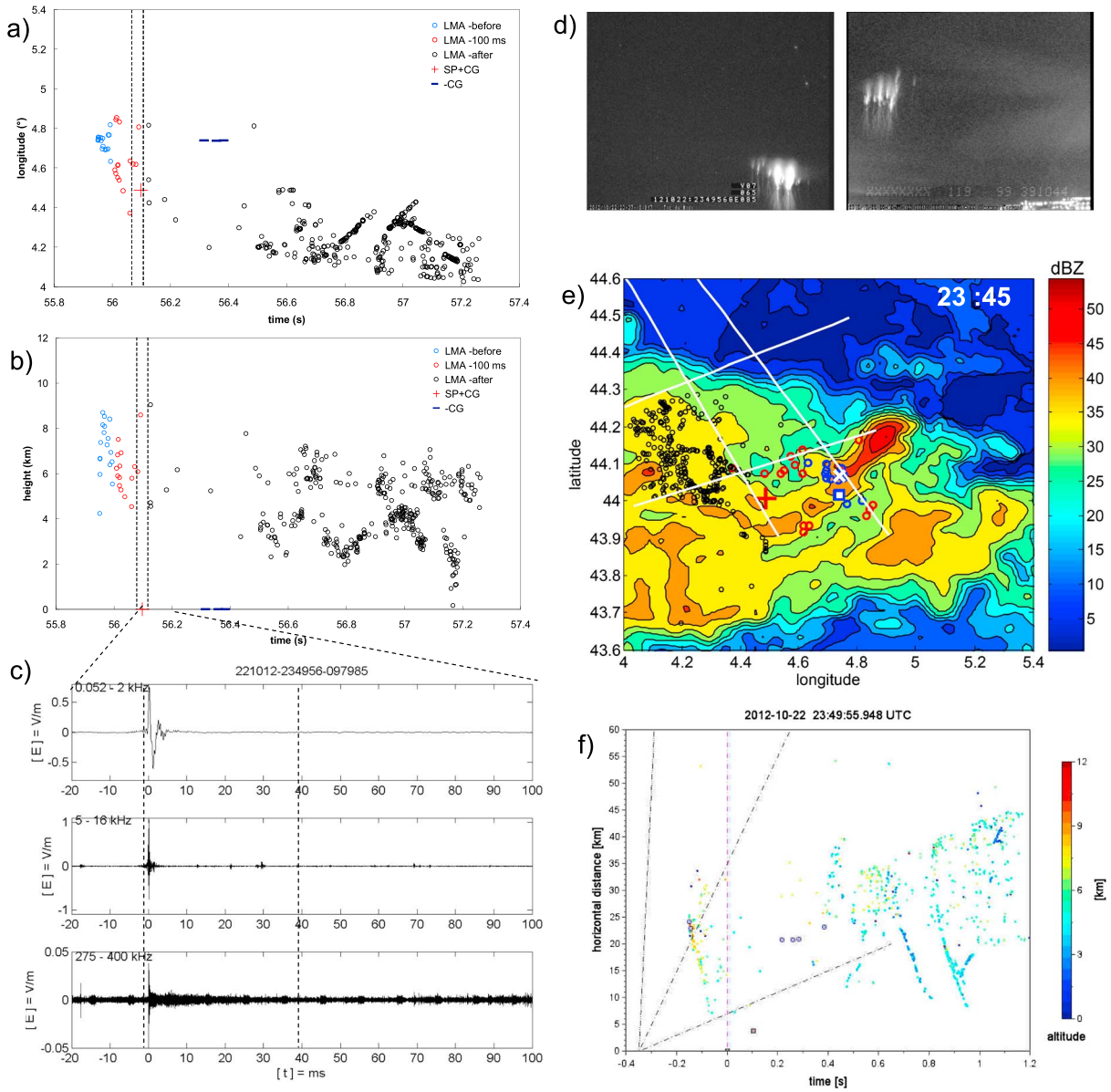


**Figure 10.** As in Figure 8 for a short delay sprite (event #5 at 2349:56 UTC). In Figure 10a and 10b time is after 2349 UTC. In Figure 10d two frames with sprite luminosity: (left) from camera 1 at $t = 56.085–105$ s and (right) from camera 2 at $t = 56.099–119$ s. In Figure 10e the reflectivity radar field is at 2345 UTC. In Figure 10f the SP + CG stroke is chosen as reference point for the distance (at $t = 0$).

be roughly estimated at about $2 \times 10^5$ m s$^{-1}$ for the first downward leader, which is typical of negative stepped leaders [*Rakov and Uman*, 2003]. Then, VHF sources are detected at two altitudes during about 0.5 s: below 5 km with slow and westward propagation, above 6 km with less density and very slow propagation. This 0.5 s sequence is dominated by a positive leader activity according to Figure 8f that shows that the VHF sources describe a time-distance characteristic of the positive leader velocity [*van der Velde and Montanyà*, 2013]. Two other −CG strokes ($t = 45.702$ s and $t = 45.766$ s with peak currents of −17 and −13 kA, respectively) are detected very close to the previous ones. Figure 8e displays the location of these sources from the first VHF source indicated by the white cross, superimposed to the radar reflectivity at 2330 UTC. At the end of this first sequence ($t \approx 45.950$ s), the VHF source locations move rapidly upward to an altitude of 11 km, as indicated in Figures 8b and 8f. The speed of this propagation ($>1.5 \times 10^5$ m s$^{-1}$) is typical of a negative leader or a leader in IC flashes [*Proctor*, 1997]. During the 100 ms preceding the sprite event, most of the VHF sources (red dots) rapidly propagate westward and downward, and a +CG stroke with

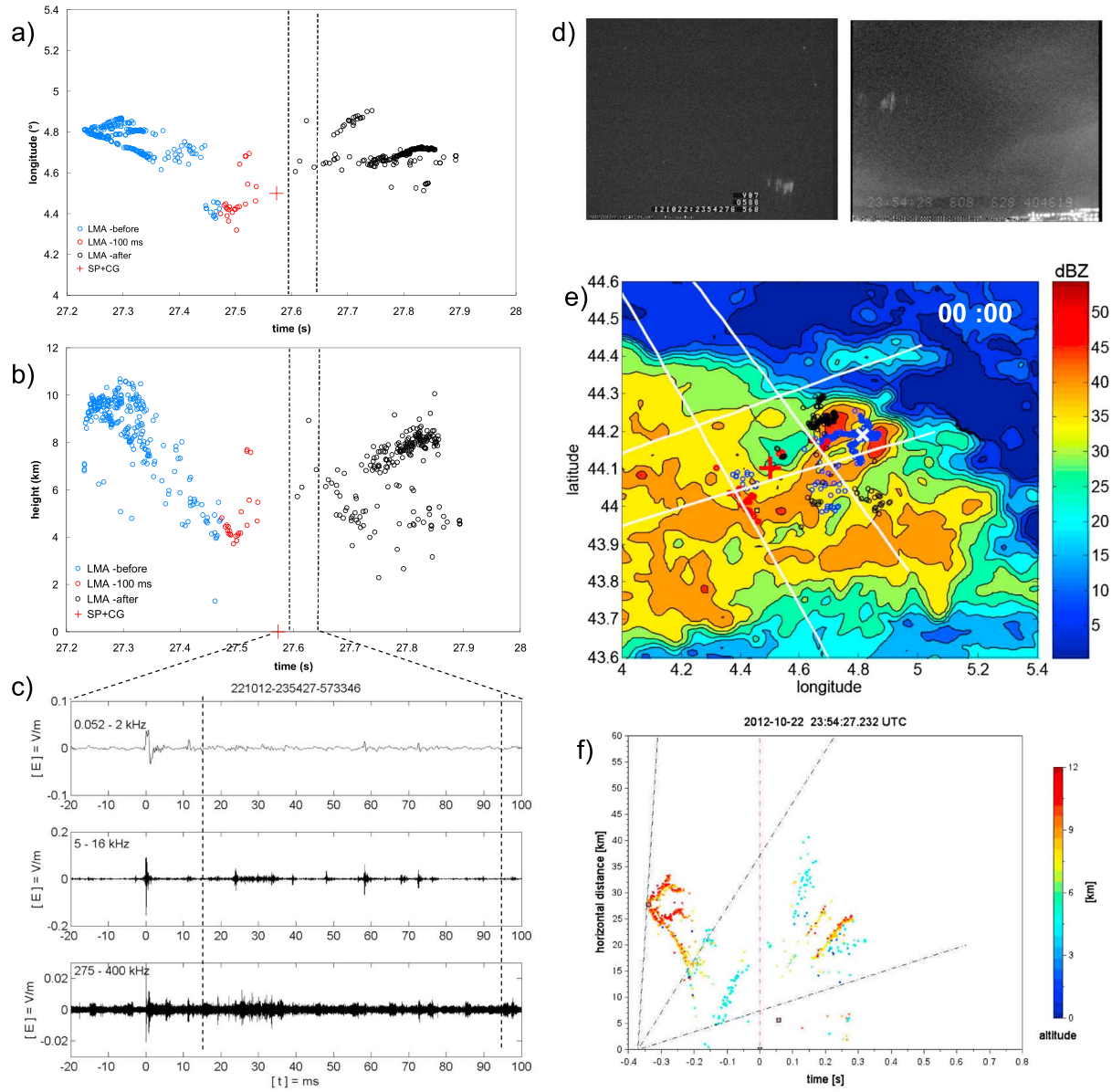


**Figure 11.** As in Figure 8 for a long delay sprite (event #6 at 2354:27 UTC). In Figures 11a and 11b time is after 2354 UTC. In Figure 11d two frames with sprite luminosity: (left) from camera 1 at $t = 27.588–608$ s and (right) from camera 2 at $t = 27.608–628$ s. In Figure 11e the reflectivity radar field is at 0000 UTC. In Figure 11f the SP + CG stroke is chosen as reference point for the distance (at $t = 0$).

a low peak current (14 kA) and a very large CMC (3086 C km) is detected at 46.112 s. These VHF sources and the +CG stroke seem to be linked. The sprite event becomes luminous during the interval $t = 46.150–46.170$ s, i.e., between 38 and 58 ms after the +CG stroke. No other +CG stroke is detected before the sprite; however, Figure 8c shows a strong activity in the VLF range with sharp pulses in the electric field at a moderate magnitude and continuous radiations typical of sferics during the luminous event (time window between the vertical dashed lines in Figure 8b). So even if very few VHF sources are reconstructed during this time window of about 60 ms, an intense activity persists in the VLF range and the LMA stations indicate also strong signal around $t = 46.150$ s. After the luminous event, the VHF sources detected by the HyLMA (black dots) are scattered in a large region of the storm and in a wide range of altitudes, as indicated in Figures 8b and 8e. Figure 8d displays two frames from camera 1 that indicated two luminous carrots in the first frame and two supplemental small columns in the second frame. Figure 8e displays the lines of view of these four elements superimposed on the VHF sources, both central lines corresponding to the sprite elements present

in the first frame in Figure 8e and both edge lines corresponding to those present in the second frame. The most luminous elements are clearly displaced (to the north) from the last VHF sources detected before the sprite event (red dots). Figure 8e shows that the lightning sequence starts close to the convective region of the storm, i.e., the core which has a radar reflectivity exceeding 50 dB$Z$ at an altitude of 3000 m, and the leader subsequently propagates throughout the stratiform region ($Z < 40$ dB$Z$). Most of VHF sources are detected in a region with reflectivity apparently lower than 40 dB$Z$.

### 4.2. Case of a Short Time-Delayed Sprite at 2333:50 UTC

Figure 9 corresponds to a short time-delayed sprite event with a double sprite emission at 2333:50 UTC (#3 in Table 1), each one associated with a SP + CG lightning stroke. Both strokes are separated by 125 ms. As in the previous case, according to Figures 9a, 9b, and 9f the first VHF sources are detected at low altitude (<6 km) in the thundercloud, some of which propagate downward and are associated with two −CG strokes at $t = 49.581$ s and $t = 49.601$ s with peak currents of −54 and −11 kA. A few tens of milliseconds later, VHF sources are detected around an altitude of 6 km. For 260 ms (from 49.610 s to 49.870 s) VHF sources are detected more and more west. According to Figure 9f the velocity of the propagation looks like that of a positive leader during this first sequence of about 0.35 s. At $t = 49.870$ s, the VHF sources rapidly propagate upward to ~11 km (with a velocity of about $3 \times 10^5$ m s$^{-1}$) and then propagate downward during 400 ms (until 50.3 s) while they move westward with increasing velocity up to ~$2 \times 10^5$ m s$^{-1}$ as indicated in Figures 9a, 9e, and 9f. During 100 ms before the first sprite event occurring between $t = 50.316$ s and $t = 50.329$ s, the VHF sources (red dots) are more scattered while most of them remain at an altitude of about 5 km (Figures 9b and 9e). The SP + CG stroke preceding the sprite event is detected at $t = 50.323$ s and located in the area below these VHF sources. This SP + CG stroke exhibits large values for peak current (76 kA), CMC (2980 C km), and iCMC (1525 C km). The sprite event consists of a group of very bright elements and long filaments (Figure 9d) that resembles to jellyfish type, located above a region where the VHF sources are widely scattered (Figure 9e). A strong electric field pulse associated with the SP + CG stroke is detected in the ELF/VLF/LF/MF range, much stronger than in the previous case as indicated in Figure 9c. During the luminous event (40 ms), no significant sferic emission is recorded while very few VHF sources are reconstructed, although the LMA stations detected strong signals. As in the previous event, the lightning flash starts close to the convective core, rapidly produces −CG strokes then goes up to an altitude of 11.5 km and propagates toward the stratiform region over an east-west distance of about 80 km (Figure 9e). Furthermore, as in the case of Figure 8, the leader process of the lightning flash accelerates in this stratiform region shortly before the luminous event occurs.

### 4.3. Case of a Short Time-Delayed Sprite at 2349:56 UTC

Figure 10 corresponds to another shortly delayed sprite event at 2349:56 UTC (#5 in Table 1). In this case, the TLE is rapidly produced after the beginning of the lightning flash that starts at $t = 55.951$ s, since the first frame with luminosity is at $t = 56.085$ s for camera 1. The first VHF source is detected at an altitude of 4.2 km while the following sources (blue dots) are rapidly detected at higher altitude up to ~9 km and more westward. During the 100 ms preceding the TLE, new VHF sources are detected at a much lower altitude (~4 km for the lower sources) and still more westward just before the sprite (Figure 10b). After the first VHF source is produced, most of the following sources occur rapidly more westward, which suggests a fast propagation (~$3 \times 10^5$ m s$^{-1}$) according to the longitude of their location displayed in Figures 10a and 10e and the time-distance graph of Figure 10f. The type of sprite corresponds to jellyfish type, of which some elements are very bright and have many long filaments. As indicated in Figure 10e, the first VHF source is produced close to the convective region of the storm system while other VHF sources are produced during about 1.3 s, before and after the SP + CG stroke at $t = 56.098$ s and scatter remotely within the stratiform region. The SP + CG stroke exhibits a large peak current (115 kA) and CMC (2348 C km). Three −CG strokes with peak currents of −36, −75, and −15 kA are detected after the SP + CG stroke and much closer to the location of the first VHF source. The ELF/VLF/LF/MF pulses corresponding to this SP + CG flash (top/middle graphs in Figure 10c) are especially strong with an electric field exceeding 0.5 V m$^{-1}$ and close to 1 V m$^{-1}$, respectively. After this strong pulse, no intense sferics are observed in VLF range, contrary to what is observed in the case of the long delayed event #2.

### 4.4. Case of a Long Time-Delayed Sprite at 2354:27 UTC

Figure 11 shows another case of a long-delayed sprite at 2354:27 UTC (#6 in Table 1). The total duration of the lightning process associated with this event is relatively short (0.65 s), and the first VHF sources are detected

**Table 2.** Characteristics of the 14 +CG Flashes (11 SP + CG Flashes and 3 +CG Flashes) and the +CG Strokes (12 SP + CG Strokes and 5 +CG Strokes)[a]

| | SP + CG Flash (11) | | | +CG Flash (3) | | |
|---|---|---|---|---|---|---|
| Characteristics | Maximum | Minimum | Average | Maximum | Minimum | Average |
| Peak current (kA) | 247 | 14 | 81 | 80 | 10 | 30 |
| CMC (C km) | 3086 | 625 | 1788 | 338 | 163 | 270 |
| iCMC (C km) | 1525 | 156 | 591 | 289 | 87 | 167 |
| Duration (s) | 2.58 | 0.66 | 1.43 | 2.18 | 0.52 | 1.11 |

[a]The peak currents, the CMC, and iCMC values are associated with the strokes.

at an altitude of about 7 km (Figure 11b) between two convective cores as indicated in Figure 11e. After the first VHF sources, other ones are rapidly detected up to an altitude of about 10 km and following several directions. One of these directions is westward after splitting at $t = 27.275$ s and subsequently moves downward to approximately 4 km, as indicated in Figures 11a, 11b, and 11f, with a velocity typical of negative leader, close to $10^5$ m s$^{-1}$ and even larger just before the SP + CG stroke. During the lightning process the SP + CG stroke is detected at $t = 27.573$ s (Figure 11a) below the stratiform region as indicated in Figure 11e where some scattered VHF sources are also detected. The peak current of the SP + CG stroke is low (16 kA), and its CMC is rather average (1629 C km). The video imagery shows several consecutive sprite elements during four successive 20 ms frames starting at $t = 27.588$ s for both cameras (Figure 11d). These elements are not very bright, and their shape is between carrot and column. The radiation produced by the SP + CG flash in the ELF/VLF/LF/MF range is much smaller in this case since the electric field recorded by the antenna does not reach 0.1 V m$^{-1}$ and 0.2 V m$^{-1}$ in ELF and VLF, respectively, as indicated by the top and middle graphs in Figure 11c. After the pulse which corresponds to the SP + CG stroke, several pulses of electric field, with a magnitude of several tens of V m$^{-1}$, occur in the VLF range, indicating a production of sferics during the 80 ms period of TLE emission (middle graph of Figure 11c).

## 5. Discussion

### 5.1. Characteristics of the Sprite-Producing Thundercloud

Twelve sprite events were observed from two sites during a period of about 1 h 30 min corresponding to the last third of the lightning activity of a storm system on the night of 22–23 October 2012. The structure and the displacement of the storm allow classifying it in a category of a leading stratiform MCS [*Parker and Johnson*, 2000]. As a matter of fact, the stratiform region develops ahead of the convective core and its area with reflectivity larger than 10 dB$Z$ is about 20,000 km$^2$ around 2330 UT when the first sprites are observed. This size has been calculated from the reflectivity values at an altitude of 3000 m displayed in Figure 7, and it corresponds to the part of the system roughly located between 3.5°E and 5.5°E in longitude. This size is relatively typical of sprite-producing storm systems according to many studies in U.S. [*Lyons et al.*, 2009]. The maximum reflectivity at 2330 UT is 56.6 dB$Z$ at this altitude of 3000 m which also corresponds very well to the value given by *Lyons et al.* [2009] for the peak core reflectivity (>55 dB$Z$) associated with the occurrence of sprites.

### 5.2. SP + CG Strokes Characteristics and Sprite Occurrence

Most SP + CG strokes are located outside of the most active region assumed to be the convective region in agreement with previous studies [*Lyons et al.*, 2009; *Lang et al.*, 2010]. The convective core of the storm is still active in terms of lightning activity, essentially with −CG flashes clustered within this core, when the first sprite is detected at 2311 UT. Between 2311 UT and the end of the lightning activity produced by this storm, 19 +CG strokes are detected by the Euclid network. Out of these 19 +CG strokes, 12 were associated with a luminous sprite event as indicated in Table 1. The peak current value for the 12 SP + CG strokes ranges between 14 and 247 kA, while the peak current for the other +CG strokes ranges between 10 and 80 kA (as indicated in Table 2). The average value of the peak current is much larger for SP + CG strokes (81 kA) compared to the other +CG strokes (30 kA). This observation matches previous observations as described, for example, in *São Sabbas et al.* [2003] and *Soula et al.* [2009]. Two SP + CG strokes are associated with the same SP + CG flash, and two +CG flashes exhibit two +CG strokes each one. Thus, the 19 +CG strokes fall into 11 SP + CG flashes and 3 +CG flashes. Table 2 displays the CMC and iCMC values for both types of +CG strokes. Thus, the CMC appears as a good predictor for the potential sprite occurrence after the +CG strokes since all

SP + CG strokes have values larger than 600 C km while all +CG strokes stay below 338 C km. This observation agrees with previous studies that showed an increase of the probability of sprites production when the CMC was larger than a threshold [*Hu et al.*, 2002; *Lyons et al.*, 2003; *Cummer and Lyons*, 2005]. The probability was, for example, 10% if the CMC was lower than 600 C km. Likewise, the iCMC values are on average much larger for SP + CG strokes, 591 C km compared to 87 C km. The range of the present CMC values is similar to those reported by *Hu et al.* [2002] for summer storms in U.S. plains or to that in *van der Velde et al.* [2014] for storms in the South of Europe. However, it is larger than that in *Matsudo et al.* [2007] for winter storms in Japan and that in *Yaniv et al.* [2014] for winter storms observed during campaigns conducted from Israel. The HyLMA data allow analyzing several characteristics of most of these flashes, especially their duration, as reported in Table 2. The duration differentiates both types of CG flash in the sense that it is longer for SP + CG flashes: on average it is 1.43 s and 1.11 s for the SP + CG flashes and the other +CG flashes, respectively.

### 5.3. SP + CG Strokes Characteristics and Sprite Luminosity

Out of the 12 sprite events recorded with the cameras, #3a and #5 are especially luminous, as displayed in Figures 9d and 10d, respectively. Both consist of multiple elements some of which are very bright, either in the main body or in the many long tendrils. According to the classification by *Bór* [2013], they correspond to jellyfish composed of several elements, in majority columns and wishbones. The SP + CG strokes of these two sprite events have the largest iCMC according to Table 1, with 1525 and 1387 C km, respectively. They have also large values of CMC. Two other sprite (#4 and #9) events are less luminous but more luminous than most of the other events. The SP + CG strokes that produced them have modest values of iCMC (898 and 728 C km, respectively) and large values of CMC (2806 and 2115 C km, respectively). On the contrary, the less bright sprites are associated with low iCMC values. The largest value of CMC corresponds with the lowest iCMC value for the event #2 that is a sprite of medium luminosity. This observation has to be compared with the study of *Yaniv et al.* [2014] in which a correlation coefficient of 0.71 was found between the sprite radiance and the CMC. A combination of both iCMC and CMC values can probably better explain the luminosity of sprites.

### 5.4. Characteristics of the Sprite-Producing Flash Processes

All the observed sprites were preceded by a +CG (SP + CG) stroke in a time delay consistent with the theory of *Pasko et al.* [1997]. The cases of negative sprites (associated with −CG strokes) are rare in the literature, and they seem to be produced by specific storms as in *Barrington-Leigh et al.* [1999] for a storm over Sea in the Gulf of California or in *Matsudo et al.* [2007] for winter storms in Japan. Some of the present SP + CG strokes are part of complex lightning processes including −CG strokes (before or/and after) and intracloud branches propagating over large distances. The HyLMA data enable a detailed analysis of the SP + CG flashes and reveal some common characteristics and some differences. All of these flashes include a +CG stroke preceding the sprite occurrence and most of them include also −CG strokes, either before the sprite or after it. Thus, most of the SP + CG flashes lower negative and positive charges to the ground. The negative charge is lowered below the region where the flash starts, always close to the convective core, while the positive charge can be lowered either close to the convective core after a −CG stroke (e.g., case of Figure 8), or below the stratiform region (e.g., other cases in Figures 9–11). After the SP + CG flash starts, several VHF sources are detected within this region and sometimes at a lower altitude (4–5 km), probably between the main negative charge within the cloud and the lower positive charge, which can generate −CG strokes as a typical −CG flash. Other VHF sources detection seem to draw slow and horizontal propagation either throughout the convective region or along it, then upward and rapid propagation at the periphery of the convective core up to 10–12 km for some cases, and finally westward propagation throughout the stratiform region with a velocity typical of a negative leader (~$2 \times 10^5$ m $s^{-1}$) progressively descending at lower altitudes. For the case of Figure 8, several successive −CG strokes weaken the main negative charge and then an upward negative leader propagates toward the positive charge above. Following this propagation, a +CG stroke detected close to the convective region lowers an amount of positive charge that is not enough to trigger the sprite. The propagation of a negative leader continues at low altitude through the stratiform region and VLF impulsive emissions show that charge is transferred before the sprite triggering that occurs with a delay between 38 and 58 s after the previous SP + CG stroke. This case of long-delayed sprite seems to correspond with the production mode #4 described in *van der Velde et al.* [2014]. For the other cases (Figures 9–11), the SP + CG

strokes are detected after a negative leader propagation over larger distances and more far away within the stratiform region. Thus, the case of Figure 9 seems to exhibit some characteristics of the short delay mode #5 in *van der Velde et al.* [2014] but with −CG strokes triggered at the beginning of the lightning process. The case of Figure 10 resembles mode #2 from van der Velde et al. because fast and short bidirectional leader propagation before the SP + CG stroke. The case of Figure 11 could resemble to their long delay mode #3 but with only one +CG stroke. According to Figures 8a, 8b, 9a, 9b, 10a, 10b, 11a, and 11b, very few VHF sources are reconstructed by the HyLMA during the time interval with sprite luminosity. However, strong VHF activity is recorded at each station within these time intervals (not shown), which requires a more detailed analysis of the data in the future. In each case of SP + CG flash, the discharge process continues after the sprite emission with leader propagation that can last up to 1 s after the SP + CG stroke, when it has been produced early in the lightning flash process.

VHF detections show that leader branches can propagate backward relative to the main westward propagation, from the first detection or from other locations on the negative leader. These other branches seem to correspond with positive leaders since it is now well known that lightning flashes triggered within the thundercloud, develop under the form of a bidirectional leader [*Kasemir*, 1960] driven by the electric field. In this description, a negative leader moves in the direction of positive charge, or through it, with stepped behavior from the initiation location where the strength of the electric field is maximum, while a positive leader moves toward negative charge and usually does not step. Then, by repetitively connecting to the positive leader tip, recoil leaders with negative polarity extend the channel retrogressively at speeds of $2 \times 10^4$ m s$^{-1}$ [*Proctor et al.*, 1988; *Shao and Krehbiel*, 1996; *Mazur*, 2002] and produce VHF sources detected by the LMA systems [*Thomas et al.*, 2001]. In the present cases, the backward (eastward) branches are associated with slower and shorter propagation, which resembles, for example, the observations made by *van der Velde and Montanyà* [2013]. As a matter of fact, these authors noted asymmetries in the bidirectional leader development in several cases of lightning flashes from observations with the Ebro 3-D Lightning Mapping Array at the east coast of Spain, combined to high-speed camera records. Thus, they found the speed of the positive leader was about 5 times smaller. The positive leader was commonly observed to move at speeds between $0.3–6 \times 10^5$ m s$^{-1}$ [e.g., *Saba et al.*, 2008], and negative leaders propagate at an average speed of $2 \times 10^5$ m s$^{-1}$ [e.g., *Mazur et al.*, 1998].

With similar data, especially from a LMA system, *Lang et al.* [2010] noted a significant proportion of cases of long-delayed sprite-producing flashes initiated in the stratiform region but in one case of a trailing stratiform MCS that produced a large number of TLEs. For a second case of a sprite-producing asymmetric MCS, Lang et al. found a very large proportion of parent lightning flashes (22 out of 23) initiated in one of the two main convective regions, i.e., in the mesoscale convective vortex and in the convective line. In the present case, the storm could be an asymmetric MCS with a low number of sprites produced which is comparable to the asymmetric MCS documented over the central U.S. by *Lang et al.* [2010]. LMA data were also used by *Lyons et al.* [2003] to document a case of a sprite-producing storm during the Severe Thunderstorm Electrification and Precipitation Study (STEPS) program. Two small MCSs produced 2 and 15 sprites, respectively, with several similar general observations compared with the present case: (i) the sprites were produced in the late mature stages of the storm, (ii) the SP + CG strokes were located within the stratiform region, and (iii) their peak currents were markedly larger than the other +CG strokes. The authors estimated the height of the positive charge layer associated with the leader propagation and the SP + CG lightning flash. They found values ranging between 2 and 5 km, with an average at 4 km above ground level. On this point our observations are consistent with theirs since for the most part, the last VHF sources before the SP + CG stroke are detected at an altitude of 4 to 5 km. Furthermore, this height did not vary much from a case to another. The positive charge involved in the SP + CG stroke is supposedly located at higher altitudes in several works, typically at 6–9 km altitude above sea level, as, for example, reported by *Stanley* [2000], *Lu et al.* [2009], and *Lang et al.* [2010]. However, the positive charge height varies among different types of storms, while the 0°C altitude can be as low as 3–5 km [*Lang et al.*, 2010] or at even lower altitude within winter storms in Japan [*Suzuki et al.*, 2011].

Figure 12 illustrates a case of +CG flash that occurs at 2315:00 UTC and does not produce any visible sprite event. The duration of this flash (2.18 s) is comparable to those of the SP + CG flashes the average of which is 1.43 s. The long distance of propagation of the flash, especially the negative leaders according to Figure 12d, corresponds also to the characteristics of the SP + CG flashes. Several negative leaders propagate successively over long distances, as indicated also in Figures 12a, 12c, and 12d. Unlike the SP + CG flash cases where the negative leaders propagate until triggering a +CG stroke, the two +CG strokes detected during this

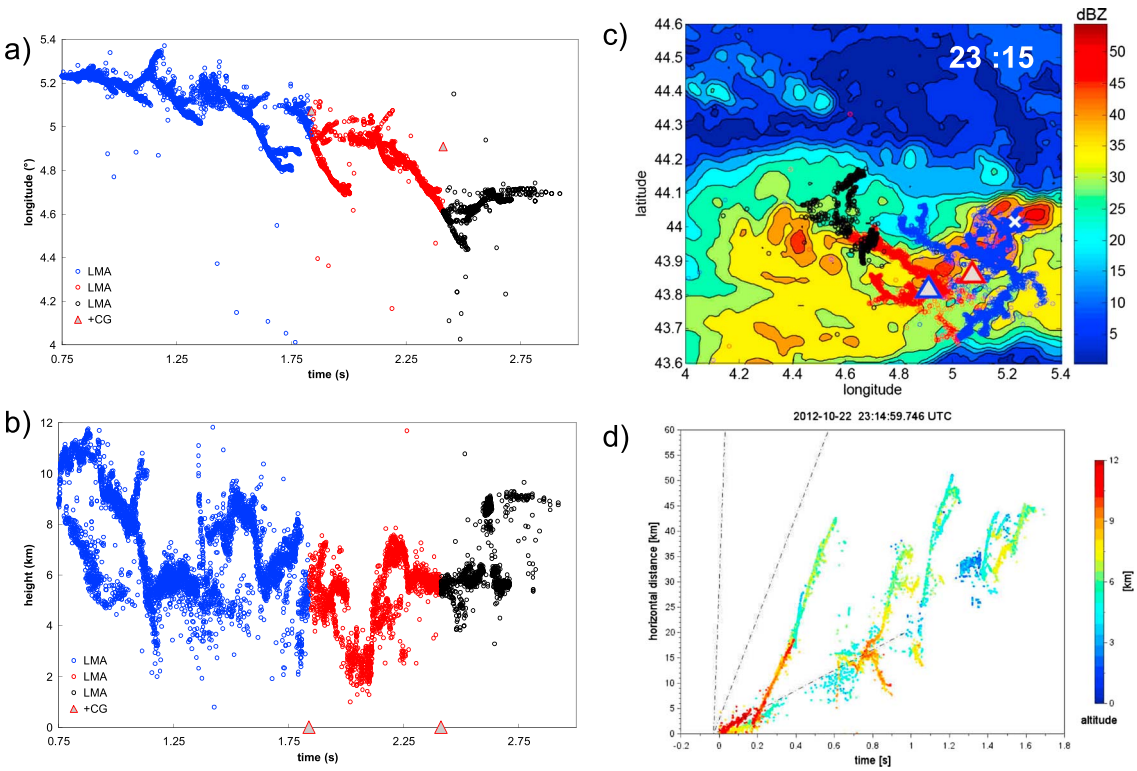


**Figure 12.** No sprite-producing +CG flash: (a) the longitude of HyLMA-detected VHF sources and Euclid-detected CG strokes versus time after 2315:00 UTC; (b) the altitude of HyLMA-detected VHF sources versus time after 2315 UTC; (c) radar reflectivity field at the altitude of 3000 m and at 2315 UTC with superimposed several events of the lightning activity associated with the sprite: the HyLMA-detected VHF sources with black symbols, the first VHF source detected indicated by the white cross, and the Euclid-detected CG strokes with grey triangle; (d) Time-distance graphs of the VHF sources, mapped by the HyLMA where the dashed reference lines indicate slopes corresponding to speeds of $2 \times 10^4$ m s$^{-1}$, $10^5$ m s$^{-1}$, and $10^6$ m s$^{-1}$. The reference location for the distance (at $t = 0$) is the initiation point of the flash.

lightning process occur early relative to the negative leader propagation. As a matter of fact, the first +CG stroke occurs at 2315:01.838 UTC while a negative leader propagates over a large distance during 0.162 s after this stroke (Figures 12a and 12d). The second +CG stroke occurs at 2315:2.411 UTC while a negative leader continues its propagation during 0.108 s after it (Figures 12a and 12d). In this case, the negative leaders do not reach the large stratiform region when the +CG strokes occur. On the other hand, the first negative leaders displayed in the graph of Figure 12d propagate over large distances but not toward the main stratiform region that develops west of the convective region. This case of flash is therefore different from the SP + CG flashes in so far as the +CG stroke occurs early relative to the propagation of a negative leader toward a reservoir of positive charge. Another case of +CG flash detected at 2302:05 UTC (not shown) illustrates the same behavior. According to several studies [*Lang et al.*, 2004, 2010; *Carey et al.*, 2005; *Lu et al.*, 2009], the production of a sprite is associated with the horizontal propagation of the negative leader through layers of positive charge carried by advection over tens of kilometers. This pattern of lightning flashes in MCSs which initiate in the convective region and follow a downward sloping pathway within the stratiform region before the +CG stroke is triggered, is favorable for sprite production.

### 5.5. Comparison of Long- and Short-Delayed Sprites

The sprite events are analyzed in detail according to their classification related to the time delay. It appears that the long delayed events may be associated with a SP + CG stroke with a low peak current, as in the sprite events #2 and #6 in Table 1. Both sprites are of carrot type, which agrees with the observations by *van der Velde et al.* [2006] that associated long delays for sprites to VLF sferic cluster before sprite triggering and to carrot shapes. Longer delays were also found for carrot sprites observed by *Matsudo et al.* [2009] over the Japan Sea. *Li et al.* [2008] attribute the triggering of long-delayed sprites to surges in long-continuing current called M components. However, two other long delay events are associated with larger peak current values,

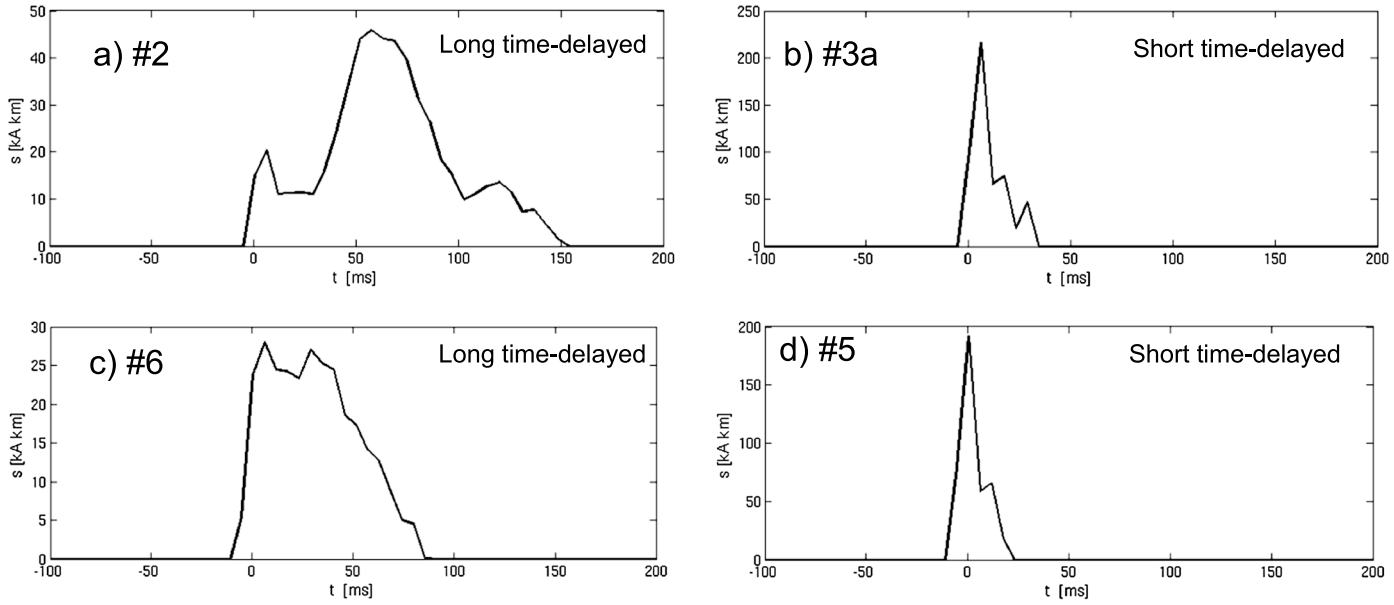


**Figure 13.** Current moment waveform recorded in Poland for the SP + CG strokes. (a and c) Long-delayed sprites (#2 at 2323:46 and #6 at 2354:27) and (b and d) short-delayed sprites (#3a at 2333:50 and #5 at 2349:56). The time $t = 0$ corresponds to the SP + CG stroke detection.

as it is visible in Table 1. First, the event #3b consists of two weakly luminous columns, produced 150 ms after a first group of very bright sprite elements and associated with a SP + CG stroke with a peak current at 75 kA south of the first SP + CG stroke at a distance of 30 km (Figure 9e). The sprite columns are also observed more in the south according to the video imagery. Second, event #10 also exhibits a long delay, but the peak current of the SP + CG stroke is very large (247 kA). In this case, a halo is seen in a first frame after the SP + CG stroke, and the sprite elements (two carrots) are observed by each camera in the following frame and in five consecutive 20 ms frames. A strong signal is recorded in the VLF range with the antenna located at Bath University, which confirms the large peak current SP + CG stroke. This sprite event has both characteristics, i.e., a long duration and a long time delay. A common characteristic of the four long-delayed sprites is a low value of the iCMC of the SP + CG stroke as indicated in Table 1. As a matter of fact, the four values range from 156 to 398 C km while the values for the other SP + CG strokes range from 255 to 1525 C km. On the contrary, the CMC values do not distinguish both types of sprites. Figure 13 illustrates the differences in terms of current moment waveform, observed between SP + CG strokes producing long and short time-delayed sprites. For long time-delayed cases (Figures 13a and 13c) the current moment signature is spread and of low amplitude (lower than 45 kA km), while for short time-delayed cases (Figures 13b and 13d) it is steep and of large amplitude (about 200 kA km). As observed and analyzed in detail by *van der Velde et al.* [2014], these long-duration current waveforms can be due to relatively weak return stroke currents and strong continuing currents. Thus, the sprite is triggered when a large amount of charge is neutralized.

## 6. Summary

During the SOP1 of the HyMeX campaign (September–November 2012), optical observations of sprite events were performed with low-light video cameras located in southern France. During the night of 22–23 October, a leading stratiform MCS developed along the coastline in southeastern France, moved westward while increasing its size up to about 20,000 $km^2$ by considering the radar reflectivity larger than 10 dB*Z*. Thanks to several lightning detection systems, especially the HyLMA that monitored the total lightning activity of the storm in three dimensions, an analysis could be performed at the scale of the overall activity during the storm lifetime and at the scale of several +CG lightning flashes, associated or not with optical observations of sprites.

The storm produces a moderate lightning activity during about 4 h, with maximum IC and CG flash rates of about 9 and 3.5 $min^{-1}$, respectively, during the first half of its lifetime. The coldest cloud top temperature (−62°C) is simultaneously observed with the maximum rate of the CG lightning flashes, most of them located

below the convective core. When the horizontal extension of this storm is maximum, during the last third of its lifetime, and while the flash rate dramatically decreases, 12 sprite events are observed over its stratiform region with one or two video cameras at distances of about 360 km and 230 km, respectively. Each sprite event is associated with a SP + CG stroke detected by the operational lightning detection network. The peak current values of these positive strokes range from 14 to 247 kA. The delay between the parent stroke and the sprite allows classifying the events within two categories, short delayed and long delayed. Some of the sprite events seen by both video cameras are triangulated. Some characteristics are inferred from the comparisons between SP + CG strokes and +CG strokes on the one hand and between long-delayed and short-delayed sprites on the other hand. (i) The CMC of the stroke is confirmed as a good predictor of the sprite production. (ii) The peak current and the iCMC are on average much larger for the SP + CG strokes. (iii) The SP + CG strokes producing long-delayed sprites have a relatively low iCMC. (iv) Long-delayed sprites, most of the time carrot sprites, are associated with current moment waveforms of low amplitude and long duration (~100 ms), VLF sferics and VHF emissions during a few tens of milliseconds after the SP + CG stroke, which shows the lightning process continues after the SP + CG stroke and can play a role in the sprite triggering.

The 3-D location of the VHF sources associated with the SP + CG flashes allows describing leader paths and their correlation with the timing and the location of the sprite elements. Furthermore, it allows analyzing some common and different features of the SP + CG flashes and other +CG flashes: (i) All SP + CG flashes initiate close to the convective core and generally generate leaders that propagate in opposite directions. One negative leader finally propagates upward close to the convective core and then propagates to lower altitudes within the stratiform region over several tens of kilometers. Other leaders remain in the initiation region with a very slow horizontal propagation, while some lead to −CG strokes. (ii) The sprite events are located above the region of the most recently produced VHF sources. These sources are scattered within the stratiform region and generally far away from where the first VHF sources of the flash sequence are detected. (iii) The +CG flashes which do not trigger a sprite emission do not propagate far away toward the stratiform region, and the +CG stroke occurs early relative to the propagation of a negative leader toward a reservoir of positive charge. They have a shorter duration in average, significantly lower peak current values.

**Acknowledgments**

The HyLMA deployment and operation were dedicated to PEACH, the Atmospheric Electricity component of HyMeX project. They were supported by the ANR IODA-MED project, and the HyLMA sensors were provided by NASA. The authors are grateful to all project participants. Observations and studies about TLEs made by S.S. were partly sponsored by the National Institute of Universe Science (INSU) thanks to LEFE/IMAGO and by the National Centre of Space Studies (CNES). Contribution from O.V. and J.M. was realized thanks to the support by the Ministry of Economy and Competitiveness (MINECO) grants AYA2011-29936-C05-04 and ESP2013- 48032-C5-3-R. All data used in this paper can be requested from the corresponding author at serge.soula@aero.obs-mip.fr.

## References

Asano, T., T. Suzuki, Y. Hiraki, E. Mareev, M. G. Cho, and M. Hayakawa (2009a), Computer simulations on sprite initiation for realistic lightning models with higher-frequency surges, *J. Geophys. Res.*, *114*, A02310, doi:10.1029/2008JA013651.

Asano, T., T. Suzuki, M. Hayakawa, and M. G. Cho (2009b), Three-dimensional EM computer simulation on sprite initiation above a horizontal lightning discharge, *J. Atmos. Sol. Terr. Phys.*, *71*(8–9), 983–990, doi:10.1016/j.jastp.2009.04.003.

Barrington-Leigh, C. P., U. S. Inan, M. Stanley, and S. A. Cummer (1999), Sprites triggered by negative lightning discharges, *Geophys. Res. Lett.*, *26*, 3605–3609.

Bell, T. F., S. C. Reising, and U. S. Inan (1998), Intense continuing currents following positive cloud-to-ground lightning associated with red sprites, *Geophys. Res. Lett.*, *25*, 1285–1288, doi:10.1029/98GL00734.

Boccippio, D. J., E. R. Williams, S. J. Heckman, W. A. Lyons, I. Baker, and R. Boldi (1995), Sprites, ELF transients and positive ground strokes, *Science*, *269*, 1088–1091.

Bór, J. (2013), Optically perceptible characteristics of sprites observed in Central Europe in 2007–2009, *J. Atmos. Sol. Terr. Phys.*, *92*, 151–177, doi:10.1016/j.jastp.2012.10.008.

Bousquet, O., and P. Tabary (2014), Development of a nationwide, real-time, 3-D wind and reflectivity radar composite in France, *Q. J. R. Meteorol. Soc.*, *140*, 611–625.

Bousquet, O., et al. (2014), Radar observations in southern France during the Hydrometeorological Cycle in the Mediterranean Experiment (HyMeX), *Bull. Am. Meteorol. Soc.*, *96*(2), 267–282, doi:10.1175/BAMS-D-13-00076.1.

Bruning, E. C., W. D. Rust, D. R. MacGorman, M. I. Biggerstaff, and T. J. Schuur (2010), Formation of charge structures in a supercell, *Mon. Weather Rev.*, *138*, 3740–3761.

Carey, L. D., M. J. Murphy, T. L. McCormick, and N. W. S. Demetriades (2005), Lightning location relative to storm structure in a leading-line, trailing-stratiform mesoscale convective system, *J. Geophys. Res.*, *110*, D03105, doi:10.1029/2003JD004371.

Cummer, S. A., and M. Füllekrug (2001), Unusually intense continuing current in lightning produces delayed mesospheric breakdown, *Geophys. Res. Lett.*, *28*, 495–498, doi:10.1029/2000GL012214.

Cummer, S. A., and U. S. Inan (1997), Measurement of charge transfer in sprite-producing lightning using ELF radio atmospherics, *Geophys. Res. Lett.*, *24*, 1731–1734.

Cummer, S. A., and W. A. Lyons (2005), Implications of lightning charge moment changes for sprite initiation, *J. Geophys. Res.*, *110*, A04304, doi:10.1029/2004JA010812.

Cummer, S. A., U. S. Inan, T. F. Bell, and C. P. Barrington-Leigh (1998), ELF radiation produced by electrical currents in sprites, *Geophys. Res. Lett.*, *25*, 1281–1284, doi:10.1029/98GL50937.

Cummins, K. L., M. J. Murphy, E. A. Bardo, W. L. Hiscox, R. B. Pyle, and A. E. Pifer (1998), A combined TOA/MDF technology upgrade of the U.S. National Lightning Detection Network, *J. Geophys. Res.*, *103*, 9035–9044.

Defer, E., et al. (2015), An overview of the lightning and atmospheric electricity observations collected in Southern France during the HYdrological cycle in Mediterranean EXperiment (HyMeX), special observation period 1, *Atmos. Meas. Tech. Discuss.*, *7*, 8013–8065, doi:10.5194/amtd-7-8013-2014.

Drobinski, P., et al. (2014), HyMeX, a 10-year multidisciplinary program on the Mediterranean water cycle, *Bull. Am. Meteorol. Soc.*, *95*(7), 1063–1082, doi:10.1175/BAMS-D-12-00242.1.

Ducrocq, V., et al. (2014), HyMeX-SOP1, the field campaign dedicated to heavy precipitation and flash flooding in the northwestern Mediterranean, *Bull. Am. Meteorol. Soc.*, *95*(7), 1083–1100, doi:10.1175/BAMS-D-12-00244.1.

Ely, B. L., R. E. Orville, L. D. Carey, and C. L. Hodapp (2008), Evolution of the total lightning structure in a leading-line, trailing stratiform mesoscale convective system over Houston, Texas, *J. Geophys. Res.*, *113*, D08114, doi:10.1029/2007JD008445.

Füllekrug, M. (2010), Wideband digital low-frequency radio receiver, *Meas. Sci. Technol.*, *21*, 015901, doi:10.1088/0957-0233/21/1/015901.

Füllekrug, M., D. R. Moudry, G. Dawes, and D. D. Sentman (2001), Mesospheric sprite current triangulation, *J. Geophys. Res.*, *106*, 20,189–20,194, doi:10.1029/2001JD900075.

Füllekrug, M., A. Mezentsev, S. Soula, O. van der Velde, and T. Farges (2013a), Sprites in low-frequency radio noise, *Geophys. Res. Lett.*, *40*, 2395–2399, doi:10.1002/grl.50408.

Füllekrug, M., A. Mezentsev, S. Soula, O. van der Velde, and A. Evans (2013b), Illumination of mesospheric irregularity by lightning discharge, *Geophys. Res. Lett.*, *40*, 6411–6416, doi:10.1002/2013GL058502.

Fuquay, D. M. (1982), Positive cloud-to-ground lightning in summer thunderstorms, *J. Geophys. Res.*, *87*, 7131–7140.

Gamerota, W., S. Cummer, J. Li, H. Stenbaek-Nielsen, R. Haaland, and M. McHarg (2011), Comparison of sprite initiation altitudes between observations and models, *J. Geophys. Res.*, *116*, A02317, doi:10.1029/2010JA016095.

Hu, W., S. A. Cummer, W. A. Lyons, and T. E. Nelson (2002), Lightning charge moment changes for the initiation of sprites, *Geophys. Res. Lett.*, *29*(8), 1279, doi:10.1029/2001GL014593.

Hu, W., S. Cummer, and W. Lyons (2007), Testing sprite initiation theory using lightning measurements and modeled electromagnetic fields, *J. Geophys. Res.*, *112*, D13115, doi:10.1029/2006JD007939.

Ignaccolo, M., T. Farges, A. Mika, T. H. Allin, O. Chanrion, E. Blanc, T. Neubert, A. C. Fraser-Smith, and M. Füllekrug (2006), The planetary rate of sprite events, *Geophys. Res. Lett.*, *33*, L11808, doi:10.1029/2005GL025502.

Kasemir, H. W. (1960), A contribution to the electrostatic theory of a lightning discharge, *J. Geophys. Res.*, *65*, 1873–1878, doi:10.1029/JZ065i007p01873.

Kosar, B., N. Liu, and H. Rassoul (2012), Luminosity and propagation characteristics of sprite streamers initiated from small ionospheric disturbances at subbreakdown conditions, *J. Geophys. Res.*, *117*, A08328, doi:10.1029/2012JA017632.

Kulak, A., J. Kubisz, S. Klucjasz, A. Michalec, J. Mlynarczyk, Z. Nieckarz, M. Ostrowski, and S. Zieba (2014), Extremely low frequency electromagnetic field measurements at the Hylaty station and methodology of signal analysis, *Radio Sci.*, *49*, 361–370, doi:10.1002/2014RS005400.

Lang, T. J., S. A. Rutledge, and K. C. Wiens (2004), Origins of positive cloud-to-ground lightning flashes in the stratiform region of a mesoscale convective system, *Geophys. Res. Lett.*, *31*, L10105, doi:10.1029/2004GL019823.

Lang, T. J., W. A. Lyons, S. A. Rutledge, J. D. Meyer, D. R. MacGorman, and S. A. Cummer (2010), Transient luminous events above two mesoscale convective systems: Storm structure and evolution, *J. Geophys. Res.*, *115*, A00E22, doi:10.1029/2009JA014500.

Li, J., S. A. Cummer, W. A. Lyons, and T. E. Nelson (2008), Coordinated analysis of delayed sprites with high-speed images and remote electromagnetic fields, *J. Geophys. Res.*, *113*, D20206, doi:10.1029/2008JD010008.

Liu, N., V. P. Pasko, H. U. Frey, S. B. Mende, H.-T. Su, A. B. Chen, R.-R. Hsu, and L.-C. Lee (2009), Assessment of sprite initiating electric fields and quenching altitude of a $^1\Pi_g$ state of $N_2$ using sprite streamer modeling and ISUAL spectrophotometric measurements, *J. Geophys. Res.*, *114*, A00E02, doi:10.1029/2008JA013735.

Lu, G., S. A. Cummer, J. Li, F. Han, R. J. Blakeslee, and H. J. Christian (2009), Charge transfer and in-cloud structure of large-charge-moment positive lightning strokes in a mesoscale convective system, *Geophys. Res. Lett.*, *36*, L15805, doi:10.1029/2009GL038880.

Lu, G., et al. (2013), Coordinated observations of sprites and in-cloud lightning flash structure, *J. Geophys. Res. Atmos.*, *118*, 6607–6632, doi:10.1002/jgrd.50459.

Lyons, W. A. (1996), Sprite observations above the U.S. High Plains in relation to their parent thunderstorm systems, *J. Geophys. Res.*, *101*, 29,641–29,652.

Lyons, W. A., T. E. Nelson, E. R. Williams, S. A. Cummer, and M. A. Stanley (2003), Characteristics of sprite-producing positive cloud-to-ground lightning during the 19 July 2000 STEPS mesoscale convective systems, *Mon. Weather Rev.*, *131*, 2417.

Lyons, W. A., M. A. Stanley, J. D. Meyer, T. E. Nelson, S. A. Rutledge, T. L. Lang, and S. A. Cummer (2009), The meteorological and electrical structure of TLE-producing convective storms, in *Lightning: Principles, Instruments and Applications*, edited by H. D. Betz et al., pp. 389–417, Springer, New York, doi:10.1007/978-1-4020-9079-0_17.

Marshall, R. A., U. S. Inan, and W. A. Lyons (2007), Very low frequency sferic bursts, sprites, and their association with lightning activity, *J. Geophys. Res.*, *112*, D22105, doi:10.1029/2007JD008857.

Matsudo, Y., T. Suzuki, M. Hayakawa, K. Yamashita, Y. Ando, K. Michimoto, and V. Korepano (2007), Characteristics of Japanese winter sprites and their parent lightning as estimated by VHF lightning and ELF transients, *J. Atmos. Sol. Terr. Phys.*, *69*(12), 1431–1446.

Matsudo, Y., T. Suzuki, K. Michimoto, K. Myokei, and M. Hayakawa (2009), Comparison of time delays of sprites induced by winter lightning flashes in the Japan Sea with those in the Pacific Ocean, *J. Atmos. Sol. Terr. Phys.*, *71*, 101–111.

Mazur, V. (2002), Physical processes during development of lightning flashes, *C. R. Phys.*, *3*, 1393–1409.

Mazur, V., X. Shao, and P. R. Krehbiel (1998), "Spider" lightning in intracloud and positive cloud-to-ground flashes, *J. Geophys. Res.*, *103*, 19,811–19,822, doi:10.1029/98JD02003.

McHarg, M. G., R. K. Haaland, D. Moudry, and H. C. Stenbaek-Nielsen (2002), Altitude-time development of sprites, *J. Geophys. Res.*, *107*(A11), 1364, doi:10.1029/2001JA000283.

Mlynarczyk, J., J. Bór, A. Kulak, M. Popek, and J. Kubisz (2015), An unusual sequence of sprites followed by a secondary TLE: An analysis of ELF radio measurements and optical observations, *J. Geophys. Res. Space Physics*, *120*, 2241–2254, doi:10.1002/2014JA020780.

Montanyà, J., O. van der Velde, D. Romero, V. March, G. Solà, N. Pineda, M. Arrayas, J. L. Trueba, V. Reglero, and S. Soula (2010), High-speed intensified video recordings of sprites and elves over the western Mediterranean Sea during winter thunderstorms, *J. Geophys. Res.*, *115*, A00E18, doi:10.1029/2009JA014508.

Neubert, T., et al. (2008), Recent results from studies of electric discharges in the mesosphere, *Surv. Geophys.*, doi:10.1007/s10712-008-9043-1.

Parker, M. D., and R. H. Johnson (2000), Organizational modes of midlatitude mesoscale convective systems, *Mon. Weather Rev.*, *128*, 3413–3436.

Pasko, V. P., U. S. Inan, T. F. Bell, and Y. N. Taranenko (1997), Sprites produced by quasi-electrostatic heating and ionization in the lower ionosphere, *J. Geophys. Res.*, *102*, 4529–4561, doi:10.1029/96JA03528.

Proctor, D. E. (1971), A hyperbolic method for obtaining VHF radio pictures of lightning, *J. Geophys. Res.*, *76*, 1478–1489.

Proctor, D. E. (1997), Lightning flashes with high origins, *J. Geophys. Res.*, *102*, 1693–1706, doi:10.1029/96JD02635.

Proctor, D. E., R. Uytenbogaardt, and B. M. Meredith (1988), VHF radio pictures of lightning flashes to ground, *J. Geophys. Res.*, *93*, 12,683–12,727.
Qin, J., S. Celestin, and V. Pasko (2012), Minimum charge moment change in positive and negative cloud to ground lightning discharges producing sprites, *Geophys. Res. Lett.*, *39*, L22801, doi:10.1029/2012GL053951.
Qin, J., S. Celestin, and V. P. Pasko (2013), Dependence of positive and negative sprite morphology on lightning characteristics and upper atmospheric ambient conditions, *J. Geophys. Res. Space Physics*, *118*, 2623–2638, doi:10.1029/2012JA017908.
Rakov, V. A., and M. A. Uman (2003), *Lightning: Physics and Effects*, Cambridge Univ. Press, New York.
Reising, S. C., U. S. Inan, T. F. Bell, and W. A. Lyons (1996), Evidence for continuing current in sprite-producing cloud-to-ground lightning, *Geophys. Res. Lett.*, *23*, 3639–3642.
Rison, W., R. J. Thomas, P. R. Krehbiel, T. Hamlin, and J. Harlin (1999), A GPS-based three-dimensional lightning mapping system: Initial observations in central New Mexico, *J. Geophys. Res.*, *26*, 3573–3576.
Rycroft, M. J., and A. Odzimek (2010), Effects of lightning and sprites on the ionospheric potential, and threshold effects on sprite initiation, obtained using an analog model of the global atmospheric electric circuit, *J. Geophys. Res.*, *115*, A00E37, doi:10.1029/2009JA014758.
Saba, M. M. F., K. L. Cummins, T. A. Warner, E. P. Krider, L. Z. S. Campos, M. G. Ballarotti, O. Pinto Jr., and S. A. Fleenor (2008), Positive leader characteristics from high-speed video observations, *Geophys. Res. Lett.*, *35*, L07802, doi:10.1029/2007GL033000.
São Sabbas, F. T., D. D. Sentman, E. M. Wescott, O. Pinto Jr., O. Mendes Jr., and M. J. Taylor (2003), Statistical analysis of space-time relationships between sprites and lightning, *J. Atmos. Sol. Terr. Phys.*, *65*, 525–535.
Sentman, D. D., and E. M. Wescott (1993), Observations of upper atmospheric optical flashes recorded from an aircraft, *Geophys. Res. Lett.*, *20*, 2857–2860, doi:10.1029/93GL02998.
Sentman, D. D., E. M. Wescott, D. L. Osborne, D. L. Hampton, and M. J. Heavner (1995), Preliminary results from the Sprites94 aircraft campaign: 1. Red sprites, *Geophys. Res. Lett.*, *22*, 1205–1208, doi:10.1029/95GL00583.
Sentman, D. D., E. M. Wescott, R. H. Picard, J. R. Winick, H. C. Stenbaek-Nielsen, E. M. Dewan, D. R. Moudry, F. T. São Sabbas, M. J. Heavner, and J. Morrill (2003), Simultaneous observations of mesospheric gravity waves and sprites generated by a Midwestern thunderstorm, *J. Atmos. Sol. Terr. Phys.*, *65*, 537–550.
Shao, X., and P. Krehbiel (1996), The spatial and temporal development of intracloud lightning, *J. Geophys. Res.*, *101*, 26,641–26,668, doi:10.1029/96JD01803.
Soula, S., O. van der Velde, J. Montanyà, T. Neubert, O. Chanrion, and M. Ganot (2009), Analysis of thunderstorm and lightning activity associated with sprites observed during the EuroSprite campaigns: Two case studies, *Atmos. Res.*, *91*(2–4), 514–528, doi:10.1016/j.atmosres.2008.06.017.
Soula, S., O. van der Velde, J. Palmieri, J. Montanya, O. Chanrion, T. Neubert, F. Gangneron, Y. Meyerfeld, F. Lefeuvre, and G. Lointier (2010), Characteristics and conditions of production of transient luminous events observed over a maritime storm, *J. Geophys. Res.*, *115*, D16118, doi:10.1029/2009JD012066.
Soula, S., F. Iacovella, O. van der Velde, J. Montanyà, M. Füllekrug, T. Farges, J. Bór, J.-F. Georgis, S. NaitAmor, and J.-M. Martin (2014), Multi-instrumental analysis of large sprite events and their producing storm in southern France, *Atmos. Res.*, *135*, 415–431, doi:10.1016/j.atmosres.2012.10.004.
Stanley, M., M. Brook, P. Krehbiel, and S. A. Cummer (2000), Detection of daytime sprites via a unique sprite ELF signature, *Geophys. Res. Lett.*, *27*, 871–874, doi:10.1029/1999GL010769.
Stanley, M. A. (2000), Sprites and their parent discharges, Ph.D. Dissertation, 163 pp., N. M. Inst. of Min. and Technol., Socorro.
Suzuki, T., Y. Matsudo, T. Asano, M. Hayakawa, and K. Michimoto (2011), Meteorological and electrical aspects of several winter thunderstorms with sprites in the Hokuriku area of Japan, *J. Geophys. Res.*, *116*, D06205, doi:10.1029/2009JD013358.
Thomas, R. J., P. R. Krehbiel, W. Rison, T. Hamlin, J. Harlin, and D. Shown (2001), Observations of VHF source powers radiated by lightning, *Geophys. Res. Lett.*, *28*, 143–146.
Thomas, R. J., P. R. Krehbiel, W. Rison, S. J. Hunyady, W. P. Winn, T. Hamlin, and J. Harlin (2004), Accuracy of the lightning mapping array, *J. Geophys. Res.*, *109*, D14207, doi:10.1029/2004JD004549.
Valdivia, J. A., G. Milikh, and K. Papadopoulos (1997), Red sprites: Lightning as a fractal antenna, *Geophys. Res. Lett.*, *24*, 3169–3172, doi:10.1029/97GL03188.
van der Velde, O. A. (2008), Morphology of sprites and conditions of sprite and jet production in mesoscale thunderstorm systems, PhD thesis, Univ. Paul Sabatier, Toulouse.
van der Velde, O. A., and J. Montanyà (2013), Asymmetries in bidirectional leader development of lightning flashes, *J. Geophys. Res. Atmos.*, *118*, 13,504–13,519, doi:10.1002/2013JD020257.
van der Velde, O. A., Á. Mika, S. Soula, C. Haldoupis, T. Neubert, and U. S. Inan (2006), Observations of the relationship between sprite morphology and in-cloud lightning processes, *J. Geophys. Res.*, *111*, D15203, doi:10.1029/2005JD006879.
van der Velde, O. A., J. Montanya, S. Soula, N. Pineda, and J. Bech (2010), Spatial and temporal evolution of horizontally extensive lightning discharges associated with sprite-producing positive cloud-to-ground flashes in northeastern Spain, *J. Geophys. Res.*, *115*, A00E56, doi:10.1029/2009JA014773.
van der Velde, O. A., J. Montanya, S. Soula, N. Pineda, and J. Mlynarczyk (2014), Bidirectional leader development in sprite-triggering lightning flashes, *J. Geophys. Res. Atmos.*, *119*, 12,755–12,779, doi:10.1002/2013JD021291.
Winckler, J. R., W. A. Lyons, T. E. Nelson, and R. J. Nemzek (1996), New high-resolution ground-based studies of sprites, *J. Geophys. Res.*, *101*, 6997–7004, doi:10.1029/95JD03443.
Yaniv, R., Y. Yair, C. Price, J. Bór, M. Sato, Y. Hobara, S. Cummer, J. Li, and A. Devir (2014), Ground-based observations of the relations between lightning charge-moment-change and the physical and optical properties of column sprites, *J. Atmos. Sol. Terr. Phys.*, *107*, 60–67, doi:10.1016/j.jastp.2013.10.018.
Yashunin, S. A., E. A. Mareev, and V. A. Rakov (2007), Are lightning M components capable of initiating sprites and sprite halos?, *J. Geophys. Res.*, *112*, D10109, doi:10.1029/2006JD007631.